

This discussion paper is/has been under review for the journal Atmospheric Measurement Techniques (AMT). Please refer to the corresponding final paper in AMT if available.

**Monitoring CO₂
emissions from
space**

H. Bovensmann et al.

A remote sensing technique for global monitoring of power plant CO₂ emissions from space and related applications

H. Bovensmann¹, M. Buchwitz¹, J. P. Burrows¹, M. Reuter¹, T. Krings¹,
K. Gerilowski¹, O. Schneising¹, J. Heymann¹, A. Tretner², and J. Erzinger²

¹Institute of Environmental Physics (IUP), University of Bremen FB1, Otto Hahn Allee 1,
28334 Bremen, Germany

²Helmholtz Centre Potsdam – GFZ German Research Centre for Geosciences,
Telegrafenberg, 14473 Potsdam, Germany

Received: 6 November 2009 – Accepted: 15 December 2009 – Published: 7 January 2010

Correspondence to: M. Buchwitz (michael.buchwitz@iup.physik.uni-bremen.de)

Published by Copernicus Publications on behalf of the European Geosciences Union.

Title Page

Abstract

Introduction

Conclusions

References

Tables

Figures

◀

▶

◀

▶

Back

Close

Full Screen / Esc

Printer-friendly Version

Interactive Discussion



Abstract

Carbon dioxide (CO₂) is the most important anthropogenic greenhouse gas causing global warming. The atmospheric CO₂ concentration increased by more than 30% since pre-industrial times – primarily due to burning of fossil fuels – and still continues to increase. Reporting of CO₂ emissions is required by the Kyoto protocol. Independent verification of reported emissions, which are typically not directly measured, by methods such as inverse modeling of measured atmospheric CO₂ concentrations is currently not possible globally due to lack of appropriate observations. Existing greenhouse gas observing satellites such as SCIAMACHY and GOSAT focus on advancing our understanding of natural CO₂ sources and sinks. The obvious next step for future generation satellites is to also measure anthropogenic CO₂ emissions. Here we present a promising satellite remote sensing technology based on spectroscopic measurements of reflected solar radiation in the short-wave infrared (SWIR) and near-infrared (NIR) spectral regions and show, using power plants as an example, that strong localized CO₂ point sources can be detected and their emissions quantified. This requires mapping the CO₂ column distribution at a spatial resolution of 2×2 km² or better with a precision of about 0.5% (2 ppm) or better of the background column. We indicate that this can be achieved with existing technology. For a single satellite in sun-synchronous orbit with an across-track swath width of 500 km each power plant is overflown every 6 days or faster. Based on clear sky statistics we conservatively estimate that about one useful measurement per 1–2 months for a given power plant can typically be achieved. We found that the uncertainty of the retrieved power plant CO₂ emission during a single satellite overpass is in the range 0.5–5 MtCO₂/year – depending on observation conditions – which is about 2–20% of the CO₂ emission of large power plants (25 Mt CO₂/year). The investigated instrument aims at fulfilling all requirements for global regional-scale CO₂ and CH₄ surface flux inverse modeling. Using a significantly less demanding instrument concept based on a single SWIR channel we indicate that this also enables the monitoring of power plant CO₂ emissions in addition

AMTD

3, 55–110, 2010

Monitoring CO₂ emissions from space

H. Bovensmann et al.

Title Page

Abstract

Introduction

Conclusions

References

Tables

Figures

◀

▶

◀

▶

Back

Close

Full Screen / Esc

Printer-friendly Version

Interactive Discussion



to high-quality methane retrievals. The latter has already been demonstrated by SCIA-MACHY. The discussed technology has the potential to significantly contribute to an independent verification of reported anthropogenic CO₂ emissions and therefore could be an important component of a future global anthropogenic CO₂ emission monitoring system. This is of relevance in the context of Kyoto protocol follow-on agreements but also allows to detect and monitor strong natural CO₂ and CH₄ emitters such as (mud) volcanoes.

1 Introduction

Carbon dioxide (CO₂) is the most important anthropogenic greenhouse gas and its atmospheric concentration increased by more than 30% since pre-industrial times and still continues to increase primarily due to burning of fossil fuels (IPCC, 2007; Canadell et al., 2007). Power plants, most notably coal-fired power plants, are among the largest CO₂ emitters (DoE and EPA, 2000). Coal-fired power plants not only emit CO₂ in large quantities but also a number of other constituents such as aerosols and ozone precursors and mercury with significant adverse influence on air quality and climate (Shindell and Faluvegi, 2009). As the world coal reserves are estimated at 930 Gt coal (see Shindell and Faluvegi, 2009, and references given therein), it can be expected that CO₂ emissions of coal-fired power plants will continue for many decades – probably with significantly growing emissions as the construction of coal-fired power plants has been increasing rapidly for example in China and India (Shindell and Faluvegi, 2009).

In many countries national legislation requires regular reporting of CO₂ emissions (e.g., DoE and EPA, 2000). Emission reporting is also required by the Kyoto protocol (<http://unfccc.int/resource/docs/convkp/kpeng.pdf>). Current CO₂ emission reporting is mostly based on economical and technical information (e.g., amount and type of fuel burned, power plant thermal efficiencies, CO₂ conversion factors) (DoE and EPA, 2000) but typically not on directly measured CO₂ emissions. Also required by the Kyoto protocol is independent verification of the reported emissions – a requirement difficult to

Monitoring CO₂ emissions from space

H. Bovensmann et al.

Title Page

Abstract

Introduction

Conclusions

References

Tables

Figures

◀

▶

◀

▶

Back

Close

Full Screen / Esc

Printer-friendly Version

Interactive Discussion



be met globally due to lack of appropriate observations. The uncertainty of the reported anthropogenic CO₂ emissions varies by sector and country. They are assumed to vary by about 3–5% for the US to 15–20% for China, which became the largest national source of CO₂ emissions during 2006 (Gregg et al., 2008).

It has been recognized that global satellite observations of the CO₂ vertical column (in molecules/cm²) or of the dry air column-averaged mixing ratio (or mole fraction) of CO₂ (in ppm), denoted XCO₂, has the potential to significantly advance our knowledge about regional natural CO₂ surface sources and sinks provided the satellite measurements have sufficiently high sensitivity to the planetary boundary layer (PBL) and are precise and accurate enough (Rayner and O'Brien, 2001; Houweling et al., 2004; Miller et al., 2007; Chevallier et al., 2007).

The dedicated greenhouse gas satellite missions Orbiting Carbon Observatory (OCO) (Kuang et al., 2002; Crisp et al., 2004; Miller et al., 2007; Chevallier et al., 2007) and Greenhouse Gases Observing Satellite (GOSAT) (Hamazaki et al., 2004) have been built to perform highly accurate and precise global PBL sensitive XCO₂ measurements. Both instruments have been designed to perform nadir mode observations (over land) and sun-glint mode observations (over ocean) of high resolution spectra in well-selected absorption bands in the short-wave infrared (SWIR) and near-infrared (NIR) spectral regions. The spectral regions covered are CO₂ absorption bands around 1.6 and 2.0 μm and the O₂-A absorption band at 0.76 μm (O₂ is included to provide additional information on clouds and aerosols and on the average surface pressure within the satellite's footprint). In contrast to OCO, GOSAT also covers absorption bands of the second most important anthropogenic greenhouse gas methane (CH₄) and also covers a large part of the thermal infrared (TIR) spectral region. GOSAT has been successfully launched in January 2009. OCO unfortunately failed during its launch in February 2009 (Palmer and Rayner, 2009).

The first satellite instrument which performed and still performs nadir measurements in the relevant spectral regions for XCO₂ and XCH₄ retrieval in the SWIR and NIR is SCIAMACHY on ENVISAT since its launch in 2002 (Burrows et al., 1995; Bovensmann

Monitoring CO₂ emissions from space

H. Bovensmann et al.

Title Page

Abstract

Introduction

Conclusions

References

Tables

Figures

⏪

⏩

◀

▶

Back

Close

Full Screen / Esc

Printer-friendly Version

Interactive Discussion



et al., 1999). XCH_4 is the dry air column-averaged mixing ratio of CH_4 (in ppb). Different groups have developed dedicated radiative transfer and CO_2 and CH_4 retrieval algorithms for SCIAMACHY and used them for the analysis of the SCIAMACHY spectral observations (Buchwitz et al., 2000a,b, 2005a,b, 2007; Frankenberg et al., 2005, 2008; Gloudemans et al., 2005; Houweling et al., 2005; Barkley et al., 2006a,b,c; Bösch et al., 2006; Schneising et al., 2008, 2009). It has been shown that SCIAMACHY can detect CO_2 variations of a few ppm, e.g., the CO_2 annual increase of about 2 ppm/year and the northern hemispheric CO_2 seasonal cycle (Buchwitz et al., 2007; Schneising et al., 2008). It has also be shown that SCIAMACHY can detect regionally elevated CO_2 over strong and extended anthropogenic source regions when averaging several years of data (Schneising et al., 2008). Until now however satellite XCO_2 retrievals have not been used for global regional-scale CO_2 surface flux inverse modeling in contrast to XCH_4 (Bergamaschi et al., 2007). The reason for this is that accurate SCIAMACHY XCO_2 retrievals are more challenging compared to XCH_4 retrievals. This is mainly because of two reasons: (i) atmospheric CH_4 at SCIAMACHY spatial resolution is typically more variable than CO_2 (about $\pm 5\%$ for XCH_4 (Bergamaschi et al., 2007; Meirink et al., 2006, 2008; Schneising et al., 2009) compared to about $\pm 2\%$ for XCO_2 (Schneising et al., 2008)) and (ii) SCIAMACHY methane retrieval suffers less from potential biases caused by light path related errors due to scattering by aerosols and residual clouds. The reason for the latter is that for XCH_4 simultaneously retrieved CO_2 columns from a near-by spectral region can be used as a proxy for the light path (“ CO_2 proxy method” first proposed by (Frankenberg et al., 2005); see also (Frankenberg et al., 2008; Buchwitz et al., 2006; Schneising et al., 2009)). Existing SCIAMACHY XCO_2 retrieval methods, which have been applied to real SCIAMACHY data, either do not consider any aerosol variability in the retrieval (Houweling et al., 2005), treat aerosol variability in a highly simplified way by using a few pre-selected aerosol scenarios (Barkley et al., 2006a,b,c, 2007) or consider aerosols and clouds indirectly by normalizing the retrieved CO_2 column by the simultaneously retrieved O_2 column from the spectrally distant O_2 -A-band using a single aerosol scenario for the radiative trans-

Monitoring CO_2 emissions from space

H. Bovensmann et al.

Title Page

Abstract

Introduction

Conclusions

References

Tables

Figures

◀

▶

◀

▶

Back

Close

Full Screen / Esc

Printer-friendly Version

Interactive Discussion



fer simulations (Buchwitz et al., 2005a; Schneising et al., 2008). The later approach is also not perfect as it suffers to some extent from the different sensitivities of the radiance spectra in the 0.76 μm (O_2) and 1.6 μm (CO_2) spectral regions with respect to aerosol and cloud effects (Schneising et al., 2008). Only recently the development of XCO₂ retrieval algorithms for SCIAMACHY started which aim at considering scattering by aerosols and (thin) clouds more explicitly (Buchwitz et al., 2009; Reuter et al., 2009).

In addition to SCIAMACHY there are other satellite instruments which measure tropospheric CO₂ in nadir mode, namely HIRS/TOVS (Chédin et al., 2002, 2003), AIRS (Engelen et al., 2004; Engelen and McNally, 2005; Chevallier et al., 2005; Aumann et al., 2005; Strow et al., 2006) and IASI (Crevoisier et al., 2009a). These sensors perform measurements in the TIR part of the electromagnetic spectrum. Nadir TIR measurements have highest sensitivity in the middle and upper troposphere but only little sensitivity for the lowest atmospheric layers, where the regional source/sink signals are largest. Their information content with respect to regional CO₂ and CH₄ sources and sinks is therefore limited and retrievals are typically restricted to the tropics because of the difficulty to separate CO₂ variations and temperature variations (Chédin et al., 2003; Engelen and Stephens, 2003; Engelen et al., 2004; Chevallier et al., 2005; Crevoisier et al., 2009a,b). Active laser based satellite systems are under study (see, e.g., Amediek et al., 2009, and references given therein) but at present no decision has been made if and when a laser based CO₂ or CH₄ satellite mission will be launched. Another promising approach is to use the complementary solar (SWIR/NIR) and thermal infrared (TIR) satellite nadir observations in combination (Christi and Stephens, 2004; Burrows et al., 2004) but also to combine passive and active (i.e., laser based) CO₂ and CH₄ instruments.

All existing CO₂ satellite sensors aim primarily at providing additional information on natural CO₂ sources and sinks. None of the existing satellite CO₂ sensors has been designed to monitor anthropogenic CO₂ emissions. In this study we present first detailed results concerning the potential to monitor strong anthropogenic CO₂ emission

Monitoring CO₂ emissions from space

H. Bovensmann et al.

Title Page

Abstract

Introduction

Conclusions

References

Tables

Figures

◀

▶

◀

▶

Back

Close

Full Screen / Esc

Printer-friendly Version

Interactive Discussion



sources such as coal-fired power plants from space. The investigated satellite mission and instrument, in the following referred to as “Carbon Monitoring Satellite” (CarbonSat), is based on the heritage of SCIAMACHY, OCO and GOSAT, but with additional (wide swath imaging) capabilities.

5 The overall scientific objectives of the hypothetical CarbonSat mission are similar as the objectives of OCO and GOSAT, namely to provide XCO₂ (and XCH₄) data products with a precision, accuracy and coverage as needed for the quantification of regional-scale CO₂ (and CH₄) surface fluxes. CarbonSat also covers absorption bands of CH₄, a very potent greenhouse gas. To also observe atmospheric methane over water, e.g.,
10 in vulnerable northern high latitude regions such as the region west of Spitsbergen (Westbrook et al., 2009) or the East Siberian Arctic Shelf area (Shakhova et al., 2009), CarbonSat is assumed to use a dedicated sun-glint observation mode, to allow high quality retrievals also over water. These aspects will however not be discussed in detail in this manuscript. Here we focus on one application, namely on the monitoring
15 of power plant CO₂ emissions from space.

The manuscript is organized as follows: in Sect. 2 we present simulations of power plant CO₂ emission plumes and discuss implications for the proposed satellite mission. In Sect. 3 we present the satellite mission concept and in Sect. 4 the satellite instrument. In Sect. 5 theoretical XCO₂ retrieval precisions are derived using a retrieval algorithm which has been applied to simulated satellite observations. In Sect. 6
20 the uncertainties of the retrieved power plant CO₂ emissions are derived based on the uncertainties of the retrieved atmospheric XCO₂. Clouds are an issue for the satellite observations. Therefore clear sky statistics are presented and discussed in Sect. 7. The findings of this study are discussed in Sect. 8. A summary and final conclusions
25 are given in Sect. 9.

Monitoring CO₂ emissions from space

H. Bovensmann et al.

Title Page

Abstract

Introduction

Conclusions

References

Tables

Figures

◀

▶

◀

▶

Back

Close

Full Screen / Esc

Printer-friendly Version

Interactive Discussion



2 Simulation of power plant CO₂ emission plumes

In order to simulate the CO₂ vertical column enhancement at and downwind of a CO₂ emitting power plant, a quasi-stationary Gaussian plume model is used, which is described in Appendix A. Figure 1 shows a typical example of a simulated CO₂ plume at high spatial resolution (left) and at a spatial resolution of 2×2 km² corresponding to the resolution of the CarbonSat satellite instrument discussed in detail below. As can be seen, the assumed CO₂ emission of 13 Mt CO₂/year results in an enhancement of the CO₂ vertical column of larger than 2% at a spatial resolution of 2×2 km² (the maximum value is 3.1% as shown in Table 1). If the ground pixel size is 10 km, which corresponds to the ground pixel size of GOSAT, the CO₂ emission only results in a CO₂ column enhancement of at most 0.5% of the background column (see Table 1). Also shown in Fig. 1 are aircraft CO₂ column retrievals performed using the Methane Airborne Mapper (MAMAP) aircraft instrument (<http://www.iup.uni-bremen.de/optronics/projects/methaneairbornemappermamap/index.htm>).

MAMAP is a spectrometer system for measuring CH₄ vertical columns or sub-columns from aircraft, which has been jointly developed by GFZ-Potsdam and IUP-Bremen (Gerilowski et al., 2009). As can be seen, MAMAP can also measure CO₂ columns. Because of this additional capability MAMAP is referred to as MAMAP/CarbonMapper in the following. MAMAP/CarbonMapper is a grating spectrometer system and covers similar spectral regions as the NIR and SWIR-1 bands of the satellite instrument discussed here (see Sect. 4).

The MAMAP/CarbonMapper results displayed in Fig. 1 are shown in more detail in Fig. 2. They are based on preliminary CO₂ and CH₄ column retrievals applied to first test data obtained during a flight with the Cessna aircraft of the Free University of Berlin (FU Berlin) over the lignite burning power plant Schwarze Pumpe located in eastern Germany near Berlin (latitude 51.54° N, longitude 14.35° E). For the time of the overflight on 26 July 2007 the CO₂ emission of Schwarze Pumpe is reported to be 13 Mt CO₂/year (Dietmar Heinze, Vattenfall Europe Generation AG & Co. KG, Cottbus,

Title Page

Abstract

Introduction

Conclusions

References

Tables

Figures

◀

▶

◀

▶

Back

Close

Full Screen / Esc

Printer-friendly Version

Interactive Discussion



Germany, personal communication, 2009).

The normalized CO_2 columns shown in Fig. 2a have been obtained by normalizing the retrieved CO_2 columns by simultaneously retrieved CH_4 columns from the same spectrometer band (“ CH_4 proxy approach”). Note that the scale used for the aircraft observations is $\pm 3\%$ compared to $\pm 2\%$ for the plume simulation. The reason for this is that the initial version of the MAMAP/CarbonMapper retrieval algorithm used here, which is a modified version of the WFM-DOAS algorithm developed for SCIAMACHY (Buchwitz et al., 2000b), overestimates the total column if the CO_2 concentration changes are restricted to near surface levels (Krings et al., 2009). The somewhat larger (colour) scale compensates for this to some extent. Figure 2b shows normalized CO_2 columns obtained by normalizing the retrieved CO_2 column by its own average (i.e., not by CH_4). As can be seen, the CO_2 enhancement due to the CO_2 emission of the power plant is also clearly visible in Fig. 2b. The CO_2 columns shown in Fig. 2b suffer to some extent from light path related errors due to, e.g., aircraft movements not yet considered in the retrieval and scattering related effects caused by the variability of aerosols and clouds, which are also not considered in the retrieval. Figure 2c shows the normalized CH_4 columns obtained by normalizing the retrieved CH_4 column by its own average, as also done for the CO_2 shown in Fig. 2b. Although the retrieved CH_4 shows significant variability, the pattern is significantly different from the CO_2 pattern. No clear correlation with the power plant location and the wind direction is visible. Assuming constant atmospheric CH_4 and noise free observations, the pattern of the retrieved CH_4 would show the light path error. As the CO_2 and CH_4 columns are retrieved using the same preliminary version of the retrieval algorithm, the columns of both retrieved gases suffer from nearly identical light path errors. Assuming constant atmospheric CH_4 over the scene of interest allows to eliminate the light path error to a large extent by normalizing the retrieved CO_2 column with the retrieved CH_4 column as done for the normalized CO_2 columns shown in Fig. 2a.

The MAMAP/CarbonMapper flight data are currently being analyzed to quantitatively determine the CO_2 emission and its associated uncertainty of the Schwarze

Monitoring CO_2 emissions from space

H. Bovensmann et al.

Title Page

Abstract

Introduction

Conclusions

References

Tables

Figures

◀

▶

◀

▶

Back

Close

Full Screen / Esc

Printer-friendly Version

Interactive Discussion



Pumpe power plant from the MAMAP/CarbonMapper spectral observations (Krings et al., manuscript in preparation). The preliminary results from the ongoing analysis does not show any significant inconsistencies between the reported power plant CO₂ emissions, the plume modelling and the aircraft observations. The MAMAP/CarbonMapper results therefore provide initial airborne demonstration for CarbonSat.

These results suggest that a satellite overpassing a given power plant can unambiguously identify power plant CO₂ emission plumes if the following conditions hold: (i) the satellite needs to have imaging capability with a spatial sampling distance and ground pixel size of about 2 km or better, (ii) the single ground pixel CO₂ column retrieval precision needs to be about 1% or better, and (iii) the satellite's swath width needs to be sufficiently large such that mapping of power plants and their surroundings with frequent overpasses can be achieved. In addition a number of other criteria need to be fulfilled. For example sufficiently cloud free conditions are needed as the satellite measures reflected solar radiation which cannot penetrate through thick clouds.

In the next section a mission concept for a single satellite is presented which has the potential to fulfill all relevant requirements for power plant CO₂ emission monitoring in addition to the requirements that need to be fulfilled for global regional-scale CO₂ and CH₄ surface flux inverse modelling (Crisp et al., 2004; Houweling et al., 2004; Miller et al., 2007; Chevallier et al., 2007).

3 Single satellite mission concept

In order to obtain frequent power plant overpasses and (nearly) global coverage within a few days with a single satellite, a low Earth orbiting (LEO) satellite mission is needed. As the satellite shall measure reflected solar radiation the sun elevation needs to be sufficiently high, i.e., the solar zenith angle (SZA) should not be too large. Assuming a sun-synchronized orbit this means that a local equator overpass time around noon would be ideal. However other aspects such as minimum cloud cover also need to be considered. In order to minimize the costs for the satellite payload it would be advanta-

Monitoring CO₂ emissions from space

H. Bovensmann et al.

Title Page

Abstract

Introduction

Conclusions

References

Tables

Figures

◀

▶

◀

▶

Back

Close

Full Screen / Esc

Printer-friendly Version

Interactive Discussion



geous to use as much as possible available relevant information from other satellites. Most important in this context is additional cloud information, in particular sub-scene (sub ground pixel) cloud information. Assuming a launch in the 2014/2015 time frame a good co-location with NPOESS C1 (launch 2014) would be a goal opportunity, primarily in order to use the relativeley high spatial resolution cloud information from the VIIRS instrument (see, e.g., <http://www.npoess.noaa.gov/>). In the following it is therefore assumed that the CarbonSat orbit is similar as the NPOESS C1 orbit (Local Time Ascending Node (LTAN) 13:30 LT repeat track 17 days). The assumed CarbonSat orbit is similar as the orbit which had been foreseen for OCO.

For the purpose of this study the scientific payload of CarbonSat is assumed to consist of a single instrument. This instrument shall be designed to measure CO₂ but also the second most important greenhouse gas methane (CH₄). The measurement precision and coverage shall be high enough to not only detect and quantify power plant CO₂ emissions but also to allow the quantification of CO₂ and CH₄ surface fluxes at about monthly time resolution at a spatial resolution of about 1000×1000 km² globally (with some likely exceptions such as the regions around the poles). The mission objectives are therefore similar as the mission objectives of OCO (Crisp et al., 2004) and GOSAT (Hamazaki et al., 2004). Compared to OCO and GOSAT, CarbonSat will however have important additional capabilities such as better spatial sampling and coverage due to the CarbonSat's wide swath imaging capabilities. Compared to OCO, CarbonSat will have a much wider swath (500 km compared to 10 km for OCO) and will also enable the retrieval of methane. This is achieved by including the relevant spectral region in the SWIR (1.6 μm) covered by methane absorption lines. In contrast to GOSAT, which has a ground pixel size of 10 km with gaps of about 150 km between the ground pixels, CarbonSat shall have a ground pixel size of 2 km and no gaps between the ground pixels (across track and along track), to allow the generation of CO₂ and CH₄ maps without gaps as needed for the unambiguous detection and subsequent quantification of CO₂ emissions by strong point sources such as power plants and volcanoes.

The global regional-scale CO₂ surface flux inverse modelling application implies de-

Monitoring CO₂ emissions from space

H. Bovensmann et al.

Title Page

Abstract

Introduction

Conclusions

References

Tables

Figures



Back

Close

Full Screen / Esc

Printer-friendly Version

Interactive Discussion



manding requirements for the satellite mission and the instrument, e.g., in terms of precision and accuracy (Houweling et al., 2004; Miller et al., 2007; Chevallier et al., 2007). For CH₄ the requirements are also high but somewhat less demanding (Meirink et al., 2006; Bergamaschi et al., 2007). These challenging requirements are considered for the instrument concept as described in the following. They are however not discussed in detail in this manuscript as the focus of this study is the assessment of CarbonSat's capability of monitor power plant CO₂ emissions.

In order to ensure frequent power plant overpasses it is important that the swath width is as large as possible. For this study we assume that the swath width will be at least 500 km. This would correspond to a full longitudinal coverage within six days at the equator and somewhat faster at higher latitudes (depending on latitude and season). Each power plant will therefore be passed at least every 6 days. For an overpass to be useful the scene needs to be sufficiently cloud free as will be discussed in below.

Figure 3 shows simulated spectra of the sun-normalized radiance as supposed to be measured by CarbonSat. The middle panel shows the relatively transparent spectral region around 1.6 μm which will deliver the main information about the CO₂ and CH₄ columns. The O₂-A-band spectral region is included to provide additional information on clouds, aerosols, and surface pressure. The right panel shows the spectral region where CO₂ has very strong absorption lines. This band will mainly be used to further reduce CO₂ retrieval errors caused by clouds and aerosols. The spectrometer system is described in more detail in the next section.

4 Instrument model

In this section a technically feasible instrument concept is described. Instrument parameters are given primarily to demonstrate that the required instrument performance can be achieved with realistic instrument parameters in line with current technology.

The instrument is assumed to be an imaging (grating) spectrometer system which

Monitoring CO₂ emissions from space

H. Bovensmann et al.

Title Page

Abstract

Introduction

Conclusions

References

Tables

Figures



Back

Close

Full Screen / Esc

Printer-friendly Version

Interactive Discussion



covers three spectral bands. Each band is covered by a Focal Plane Array (FPA) which is assumed to consist of at least 1000 spectral detector pixels times at least 250 spatial detector pixels.

The signal-to-noise ratio of the three bands determines to a large degree if the power plant emission signals can be detected. To estimate the signal-to-noise ratio (SNR) using radiance spectra and given instrument parameters a simple but realistic instrument model is used. The SNR is defined as follows:

$$\text{SNR} = \frac{S}{N}, \quad (1)$$

where S is the measured signal (in electrons). S is the “atmospheric” signal after calibration, i.e., after subtraction of the signal generated by the instrument. N is the noise (in electrons root mean square (r.m.s.)). The signal S is computed as follows:

$$S = L \times \tau \times \text{QE} \times A_{\text{det}} / F_{\text{num}}^2 \times \Delta\lambda \times N_{\text{sr}} \times t_{\text{int}}, \quad (2)$$

where L is the observed radiance (in photons/s/nm/cm²/steradian), τ is the throughput or transmission of a channel, and QE is the detector quantum efficiency. $\Delta\lambda$ is the spectral bandwidth (in nanometer) corresponding to a given detector pixel, which is equal to the spectral resolution Full Width at Half Maximum (FWHM) of the instrument line shape function divided by the spectral sampling ratio N_{sr} , i.e., the number of detector pixels per FWHM. A_{det} is the detector pixel area, F_{num} is the F -number of the spectrometer, and t_{int} is the integration or exposure time.

Note that the term $A_{\text{det}} / F_{\text{num}}^2 \times \Delta\lambda \times N_{\text{sr}}$ is equivalent (equal) to $A_{\text{ap}} \times \Omega \times \Delta\lambda / N_{\text{sr}}$, where, A_{ap} is the spectrometer aperture area and Ω is the spectrometer acceptance (solid) angle. The product $A_{\text{ap}} \times \Omega$ is typically referred to as etendue. Ω is determined by the ground pixel size and the orbit altitude. A_{ap} needs to be chosen sufficiently large to ensure an appropriate instrument performance, e.g., in terms of the required signal to noise ratio. Alternatively, the instrument can be specified by its F -number, F_{num} , which needs to be chosen sufficiently small to get the desired performance.

Monitoring CO₂ emissions from space

H. Bovensmann et al.

Title Page

Abstract

Introduction

Conclusions

References

Tables

Figures

◀

▶

◀

▶

Back

Close

Full Screen / Esc

Printer-friendly Version

Interactive Discussion



Monitoring CO₂ emissions from space

H. Bovensmann et al.

Title Page

Abstract

Introduction

Conclusions

References

Tables

Figures

◀

▶

◀

▶

Back

Close

Full Screen / Esc

Printer-friendly Version

Interactive Discussion



The noise N consists of four terms, the atmospheric signal shot noise term (\sqrt{S}), the detector dark signal shot noise term ($\sqrt{S_{\text{dark}}}$), the thermal background radiation signal shot noise term ($\sqrt{S_{\text{back}}}$) and the electronic readout noise term N_{read} :

$$N = \sqrt{S + S_{\text{dark}} + S_{\text{back}} + N_{\text{read}}^2} \quad (3)$$

The dark signal S_{dark} (in electrons) is computed as follows:

$$S_{\text{dark}} = I_{\text{dark}} \times t_{\text{int}}, \quad (4)$$

where I_{dark} is the dark current in Ampere. The signal caused by the thermal background radiation of the instrument, S_{back} (in electrons), is given by:

$$S_{\text{back}} = I_{\text{back}} \times t_{\text{int}}, \quad (5)$$

where I_{back} is the background signal in Ampere.

Realistic numerical values of these parameters are listed in Table 2. along with the resulting SNR for nine scenarios. FPA's for the NIR and SWIR spectral regions are available from several manufacturers based on different technologies. It is not the intention of this study to investigate in detail the performance of specific existing devices. Instead typical performance parameters are used. Several manufacturers offer NIR and SWIR FPA's with 1024 times 256 detector pixels, which are appropriate for the application investigated here. The sizes of the individual detector pixels are similar as the size used here ($24 \mu\text{m} \times 24 \mu\text{m}$). The values used here for the readout noise are on the order of the values given by different manufacturers. This is also true for the assumed quantum efficiency. The dark current significantly depends on the operating temperature of the detector. It is assumed here that a temperatur low enough is used to ensure sufficiently low dark signal (the default value assumed here is 3 fA for the SWIR bands). The thermal background signal depends on the temperature of the optical bench. A low enough temperature of the optical bench is critical especially for the long wavelength band SWIR-2. It is assumed that the optical bench temperature

will be low enough to achieve a good performance (the default value used here is 2 fA). The values assumed here for the optical throughput τ are also realistic (V. Mogulsky, Kayser-Threde GmbH, personal communication). The F -number is chosen to be 2, which is close to the F -number used for OCO.

5 Nine scenarios have been defined for the simulations. They differ in surface albedo and solar zenith angle (SZA) as can be seen from Table 2. These are the two most important parameters which determine the radiance level and therefore the SNR or its inverse, the relative spectral radiance measurement error. An overview about the scenarios is given in Table 3. Surface spectral albedos of different surface types are shown
10 in Fig. 5. Different wavelength dependent surface albedos have been defined for the scenarios corresponding to vegetation (“VEG” scenarios) and sand / soil (“SAS” scenarios) land surfaces. In addition, scenarios with a constant surface albedo have been defined including one scenario with very low albedo corresponding to water (“WAT”).

In (Bösch et al., 2006), SNR values for OCO are listed for a scenario with an albedo
15 of 0.05 and a solar zenith angle of 60° which can be compared with the SNRs listed in Table 2 for the A005_60 scenario. For the O₂-A-band (NIR band) the reported SNR for OCO is 360 (here: 220), for the weak CO₂ band (SWIR-1) the OCO SNR is 250 (here: 220), and for the strong CO₂ band (SWIR-2) the OCO SNR is 180 (here: 50). This indicates that the instrument parameters assumed here are conservative and can
20 probably be optimized in order to achieve a signal-to-noise performance as has been specified for OCO.

The signal and the SNR for the vegetation scenario with a SZA of 25° are shown in Fig. 6. The SNR is important as it determines the retrieval precision of the atmospheric parameters. How the CO₂ retrieval precision is obtained from the simulated signal and
25 its error (inverse SNR) is described in the next section.

Monitoring CO₂ emissions from space

H. Bovensmann et al.

Title Page

Abstract

Introduction

Conclusions

References

Tables

Figures



Back

Close

Full Screen / Esc

Printer-friendly Version

Interactive Discussion



5 Simulation of satellite observations and CO₂ retrieval

In order to estimate the CO₂ column retrieval precision given the measured spectrum and its error an Optimal Estimation (OE) retrieval algorithm is used. The underlying theory is described in detail in (Rodgers, 2000). The algorithm used is an initial implementation of a new algorithm which is under development for improved SCIAMACHY CO₂ retrieval, and is referred to as “Bremen optimal ESTimation DOAS” (BESD) (Buchwitz et al., 2009; Reuter et al., 2009). Below we give a short description of BESD. A detailed description is given in Appendix B.

CarbonSat is assumed to measure radiance spectra $L_i \equiv L(\lambda_i)$ in nadir mode at discrete wavelengths λ_i as well as the solar irradiance, $F_i \equiv F(\lambda_i)$. From these two quantities the (measured) sun-normalized radiance or intensity I_i can be computed: $I_i \equiv \pi R_i / F_i$. Measurement vector \mathbf{y} has elements $y_i \equiv \ln(I_i)$. The corresponding model quantity \mathbf{y}^{mod} is obtained with the radiative transfer model (RTM) SCIATRAN (Buchwitz et al., 2000a; Rozanov et al., 2002). It is assumed that the radiative transfer (RT) is sufficiently linear so that the logarithm of the sun-normalized radiance can be linearized around an assumed (atmospheric) state denoted by the a priori state vector \mathbf{x}_a . This means that we assume that the following equation holds for \mathbf{y}^{mod} as a function of state vector \mathbf{x} :

$$\mathbf{y}^{\text{mod}}(\mathbf{x}) = \mathbf{y}_a + \mathbf{K}(\mathbf{x} - \mathbf{x}_a). \quad (6)$$

Here $\mathbf{y}_a \equiv \mathbf{y}^{\text{mod}}(\mathbf{x}_a)$, i.e., \mathbf{y}_a is the logarithm of the intensity for state vector \mathbf{x}_a . Matrix \mathbf{K} contains the derivatives of the logarithm of the intensity with respect to the state vector elements and is typically referred to as Jacobian matrix.

BESD is based on minimizing the following cost function $C(\mathbf{x})$:

$$C(\mathbf{x}) = (\mathbf{x} - \mathbf{x}_a)^T \mathbf{S}_{x_a}^{-1} (\mathbf{x} - \mathbf{x}_a) + (\mathbf{y} - \mathbf{y}^{\text{mod}}(\mathbf{x}))^T \mathbf{S}_y^{-1} (\mathbf{y} - \mathbf{y}^{\text{mod}}(\mathbf{x})). \quad (7)$$

Here \mathbf{S}_{x_a} is the a-priori uncertainty (or variance/covariance) matrix of state vector \mathbf{x}_a . \mathbf{S}_y is the measurement error variance/covariance matrix. $()^T$ denotes matrix transpose

Title Page

Abstract

Introduction

Conclusions

References

Tables

Figures

◀

▶

◀

▶

Back

Close

Full Screen / Esc

Printer-friendly Version

Interactive Discussion



and $()^{-1}$ denotes matrix inverse. The solution of this estimation problem is an estimate of the state vector, \hat{x} , and its variance/covariance matrix $\hat{\mathbf{S}}_x$. How this solution can be obtained is described in Appendix B.

The columns of the Jacobian matrix \mathbf{K} for a typical RT simulation are shown in Fig. 7. Each column of \mathbf{K} corresponds to one state vector element. The state vector elements and their assumed a-priori uncertainties are listed in Table 4. For the retrieval a 3-layer atmosphere is used (the RT simulations are however performed on a finer vertical grid). The three layers are denoted “Lower Troposphere” (LT), “Upper Troposphere” (UT), and “Stratosphere” (ST). As can be seen from Table 4, 21 state vector elements have been defined. For CO_2 and CH_4 their sub-columns (layer columns) in the three atmospheric layers are state vector elements. For each of the three layers a dimensionless scattering parameter has been defined, the layers aerosol and cloud scattering (ACS) optical depth. Additional parameters are scaling factors for the temperature (TEM) and water vapour (H_2O) vertical profiles, a scaling parameter for the pressure profile (“surface pressure” parameter PSU) and nine parameters for the three second order polynomials in the three spectral bands (parameters POL). The Optimal Estimation method requires a-priori uncertainties to be assigned to each parameter and the corresponding values, which are to be interpreted as 1-sigma relative uncertainties, are also listed in Table 4. The two variance/covariance matrices \mathbf{S}_{x_a} and \mathbf{S}_y are assumed to be diagonal matrices, i.e., they are fully specified by the uncertainties (standard deviations) listed in Table 4.

For the retrieval two CO_2 mixing ratio profiles have been defined. The a-priori CO_2 profile has a constant mixing ratio of 390 ppm. For the simulated measurements the CO_2 profile has been enhanced in the lowest few hundred meters of the atmosphere. This enhancement is assumed to be caused by the power plant CO_2 emission at some distance downwind from the location of the power plant. The two profiles are shown in Fig. 8 along with the numerical values of the corresponding CO_2 and dry air vertical columns and XCO_2 . For this study the focus is on the achievable CO_2 column and XCO_2 retrieval precisions, which are defined as the statistical uncertainty of the re-

Monitoring CO_2 emissions from space

H. Bovensmann et al.

Title Page

Abstract

Introduction

Conclusions

References

Tables

Figures

◀

▶

◀

▶

Back

Close

Full Screen / Esc

Printer-friendly Version

Interactive Discussion



trieved quantities due to instrument noise. The main results presented here are nearly independent of the assumed CO₂ vertical profile. The retrievals based on the CO₂ profile with the enhanced mixing ratios close to the Earth's surface has only be selected to demonstrate that the satellite measurements are in fact highly sensitive to CO₂ variations close to the Earth surface which is a necessary condition for the monitoring of power plant CO₂ emissions.

Of concern are of course not only random errors but also systematic errors, e.g., due to clouds and aerosols. It is assumed that only sufficiently cloud free scenes are useful for the application discussed here. Furthermore, the BESD retrieval algorithm accounts to some extent for disturbing scattering effects due to residual (very thin and/or very small, i.e., sub-pixel) clouds and aerosols. This is done by exploiting the information content of the three spectral regions, in particular the two spectral regions covered by the NIR and the SWIR-2 bands (Kuang et al., 2002). Additional very useful information can be obtained from the simultaneously retrieved methane column using its absorption lines located next to the CO₂ lines in band SWIR-1 as the retrieved methane column will suffer from similar scattering related errors as the retrieved CO₂ column (Schneising et al., 2008, 2009). This can be used to identify and (partially) correct scattering related biases similar as done for SCIAMACHY methane retrieval (Schneising et al., 2009). This requires that the methane variability is negligible compared to the variability of CO₂ (in terms of the relative enhancement of the vertical column) as will typically be the case for the main application discussed here. This has been confirmed by MAMAP/CarbonMapper aircraft observations near power plants (Krings et al., manuscript in preparation) as discussed earlier.

Retrieval results for the VEG₂₅ scenario (vegetation albedo and SZA 25°) are shown in Fig. 9. As can be seen, a significant uncertainty reduction relative to the assumed a-priori uncertainty has been achieved for the tropospheric layers, especially for the lowest tropospheric layer (the stratospheric layer is well constrained). The true CO₂ vertical column is 8.609×10^{21} molecules/cm², which is 1.96% higher than the a-priori column, which is 8.432×10^{21} molecules/cm². The retrieved CO₂ vertical column is

Monitoring CO₂ emissions from space

H. Bovensmann et al.

Title Page

Abstract

Introduction

Conclusions

References

Tables

Figures

◀

▶

◀

▶

Back

Close

Full Screen / Esc

Printer-friendly Version

Interactive Discussion



Monitoring CO₂ emissions from space

H. Bovensmann et al.

Title Page

Abstract

Introduction

Conclusions

References

Tables

Figures

◀

▶

◀

▶

Back

Close

Full Screen / Esc

Printer-friendly Version

Interactive Discussion



8.602×10^{21} molecules/cm², which is nearly identical with the true column. The difference is -0.08% , i.e., not zero, e.g., because of the smoothing error (see Appendix B), which is 0.13% (1-sigma). The a-priori CO₂ column uncertainty is 3.62% and is reduced to 0.26% after the retrieval. The assumed a-priori surface pressure uncertainty is 3.0% and is reduced to 0.11% after the fit. The a-posteriori XCO₂ uncertainty is 1.1 ppm. The degree of freedom for signal (ds , see Appendix B) is 1.26 for the CO₂ column and 1.23 for the CH₄ column, which indicates that essentially only vertical column information on CO₂ and CH₄ is available. The CO₂ column averaging kernel is approximately unity for the lowest layer indicating that the observing system is very sensitive to CO₂ changes in the lowest atmospheric layer, which is also true for CH₄. The two panels at the bottom right, which show the results for the scattering profile, indicate significant uncertainty reduction with respect to the aerosol and cloud scattering parameters. The key results of the retrieval using the VEG₂₅ scenario are listed in Table 3 along with the corresponding results for the other scenarios.

As can be seen from Table 3, the statistical uncertainty of the retrieved XCO₂ is in the range $1\text{--}2$ ppm ($0.25\text{--}0.5\%$) for the land scenarios.

Uncertainties of the retrieved atmospheric CO₂ result in uncertainties of the inferred power plant CO₂ emission. How these emission uncertainties can be estimated is described in the next section.

6 Uncertainty of the retrieved power plant CO₂ emissions

Given a map of the retrieved XCO₂ or of the retrieved CO₂ column around a power plant and their associated retrieval uncertainties, the resulting uncertainty of the retrieved power plant CO₂ emission can be estimated. For this purpose the quasi stationary Gaussian plume forward model already presented in Sect. 2 is used in combination with a weighted linear least-squares inversion method. The results are summarized in Table 5.

As can be seen from Table 5, a single ground pixel XCO₂ measurement error of 1--

Monitoring CO₂ emissions from space

H. Bovensmann et al.

Title Page

Abstract

Introduction

Conclusions

References

Tables

Figures



Back

Close

Full Screen / Esc

Printer-friendly Version

Interactive Discussion



2 ppm results in an uncertainty of the inferred power plant CO₂ emissions in the range 0.5–5 MtCO₂/year, depending on observation conditions. The CO₂ emission uncertainty is nearly independent of the absolute value of the CO₂ emission but depends nearly linearly on wind speed. Horizontal wind speeds larger than 4 m/s (14.4 km/h) could result in uncertainties larger than 5 MtCO₂/year. Most of the observations will however be carried out under cloud free conditions, which typically corresponds to relatively stable fair weather conditions with low wind speeds.

An uncertainty of 0.5–5 Mt CO₂/year corresponds to about 2–20% of the CO₂ emission of large power plants (order 25 Mt CO₂/year, see Table 6). This uncertainty is the statistical error of the inferred power plant CO₂ emission due to the statistical uncertainty of the retrieved CO₂ columns or XCO₂ over and around a given power plant. The overall error is however larger if also other error sources are considered, for example, the uncertainty in the knowledge of the wind field. For the Gaussian plume model it can be shown that the relative uncertainty of the strength of the wind results in a similar error of the emission flux, i.e., a 10% error of the magnitude of the wind results in a 10% error of the retrieved CO₂ emission. Uncertainties in the wind direction also result in an error of the retrieved power plant CO₂ emission. This error is most likely not a dominating error source as information on the wind direction can be obtained from the satellite observation thanks to the plume mapping capability.

The 0.5–5 MtCO₂/year CO₂ emission uncertainty corresponds to a single power plant overpass. In order to determine how many useful measurements can be obtained in a given time period it needs to be investigated how many sufficiently cloud free overpasses are to be expected. This aspect is discussed in the next section.

7 Clear sky statistics for power plant overpasses

The satellite observations are based on reflected solar radiation, which cannot penetrate through thick clouds. Therefore sufficiently cloud free scenes are needed. To determine the probability for sufficiently cloud free scenes for the power plant over-

passes, one year of high resolution (1 km) global MODIS/Aqua Collection 5 Level 2 Cloud Mask data products (Ackermann et al., 1998, 2008; Frey et al., 2008) have been analyzed. MODIS/Aqua has essentially the same orbit as assumed here for Carbon-Sat (sun-synchronous, Local Time Ascending Node (LTAN) 13:30), i.e., MODIS/Aqua is therefore well suited for this application.

Figure 10 shows the resulting clear sky probabilities for the year 2008. The clear sky probabilities shown are valid for 16 km×16 km large scenes, i.e., for given (power plant) locations and their surrounding. As the MODIS/Aqua cloud masking algorithm is very strict, the results presented here are quite conservative. It is likely that also scenes with partial cloud cover can be used for power plant emission monitoring. It needs to be investigated in a future study to what extent the strict filtering criteria used here can be relaxed to increase the number of useful observations.

Also shown in Fig. 10 are the locations of several power plants and the clear sky probability at their location. The numerical values are also listed in Table 6 along with the clear sky probabilities for the four seasons. The power plant names, locations and CO₂ emissions have been obtained from the CARMA data base (<http://carma.org>).

As can be seen, on average about 20% of the satellite overpasses over the power plants correspond to clear sky conditions. Depending on power plant the clear sky probability may significantly depend on the season.

8 Discussion of the results

The results presented show that the investigated satellite permits to measure the CO₂ emission of power plants with an uncertainty of about 0.5–5 Mt CO₂/year during each overpass if the scene is sufficiently cloud free. It has been shown that on average about 20% of the overpasses fulfill this condition. For some power plants however only about 10% or even less of the observations are strictly cloud free. Taking into account that full longitudinal coverage is achieved after 6 days this shows that on average about once per 1–2 months a useful measurement of the CO₂ emission of a given power plant

Monitoring CO₂ emissions from space

H. Bovensmann et al.

Title Page

Abstract

Introduction

Conclusions

References

Tables

Figures



Back

Close

Full Screen / Esc

Printer-friendly Version

Interactive Discussion



can be achieved. The satellite therefore permits to detect strong CO₂ emitters such as power plants, but also other strong localized CO₂ sources such as volcanoes, whose CO₂ emissions are much less known compared to power plant emissions. Similar remarks apply to strong methane emission sources such as mud volcanoes and pipeline leaks.

The requirements on the performance of the satellite are similar as the requirements identified for OCO and GOSAT in terms of, e.g., spectral coverage, signal-to-noise performance and retrieval precision. The studied satellite mission is therefore supposed not only to monitor the greenhouse gas emission of point sources but to also deliver XCO₂ and XCH₄ retrievals with the precision, accuracy and coverage needed for inverse modeling of CO₂ and CH₄ surface fluxes. Especially for CO₂ this requires to meet challenging accuracy requirements. Regional biases caused by, e.g., scattering due to aerosols and clouds, need to be very small (well below 1%) as otherwise the spatio-temporal variations of the retrieved XCO₂ can be misinterpreted. The global regional-scale CO₂ surface flux inversion application is therefore the driver for the requirements the satellite has to meet. For the applications discussed in this manuscript however also a less challenging (and therefore less expensive) instrument concept is very likely feasible.

This simpler instrument would consist of only one spectral band (spectrometer), namely the SWIR-1 band which covers the weak CO₂ and CH₄ absorption bands. For the detection and monitoring of power plant CO₂ emissions the vertical columns of CO₂ and CH₄ need to be retrieved from the SWIR-1 band as done for SCIAMACHY XCH₄ retrieval using a similar spectral region (Frankenberg et al., 2005, 2008; Buchwitz et al., 2006; Schneising et al., 2009), albeit at much higher spatial resolution (2 km×2 km for CarbonSat compared to 60 km×30 km for SCIAMACHY). In the vicinity of strong CO₂ point sources, such as power plants, one can savely assume that CH₄ is much less variable compared to CO₂. Therefore the dry air column needed to compute XCO₂ can be obtained from the retrieved CH₄ column. This “CH₄ proxy” approach is similar as the “CO₂ proxy” method used for SCIAMACHY XCH₄ retrieval (Frankenberg et al.,

Monitoring CO₂ emissions from space

H. Bovensmann et al.

Title Page

Abstract

Introduction

Conclusions

References

Tables

Figures

◀

▶

◀

▶

Back

Close

Full Screen / Esc

Printer-friendly Version

Interactive Discussion



2005, 2008; Buchwitz et al., 2006; Schneising et al., 2009). Essentially the only difference is that the inverse ratio is used (i.e., CO_2/CH_4 instead of CH_4/CO_2). As has been demonstrated for SCIAMACHY methane retrieval, light path related errors will cancel to a large extent when the CO_2 to CH_4 column ratio (or its inverse) is computed.

5 This relative measurement approach ensures high relative accuracy of the resulting XCO_2 data product. Using only the SWIR-1 band would result in a somewhat worse CO_2 column retrieval precision as the CO_2 information from the SWIR-2 band would not be available any more. The impact is however only marginal. For example for the VEG_50 scenario the CO_2 column uncertainty would increase from 0.28% to 0.32%.
10 For the methane columns the uncertainties are essentially identical as neither the NIR band nor the SWIR-2 band contains significant information on the methane column. This compact version of CarbonSat (“CarbonSat/C”) would therefore likely fulfill many of the scientific objectives of the 3-band CarbonSat instrument, except at least one major objective, namely to provide the necessary data for the determination of global regional-scale CO_2 surface fluxes.
15

CarbonSat is also potentially well suited to detect and monitor many other strong greenhouse gas hot spot emission sources, e.g., CO_2 emissions from volcanoes (see, e.g., Spinetti et al., 2008, and references given therein) or CH_4 emissions from a large number of anthropogenic sources such as methane emissions from pipeline leaks
20 (Lelieveld et al., 2005), abandoned but not closed gas wells (Rehder et al., 1998), and actively exploited gas fields (Jagovkina et al., 2000) as well as natural marine and terrestrial strong or potentially strong localized or extended geological sources such as mud volcanoes, methane seeps or destabilizing continental margin methane hydrates (Dimitrov, 2002; Kourtidis et al., 2006; Leifer et al., 2006a,b; Baicu et al., 2007; Etiope, 2009; Etiope et al., 2009; Solomon et al., 2009; Shakhova et al., 2009; Westbrook et al., 2009).
25

Monitoring CO_2 emissions from space

H. Bovensmann et al.

Title Page

Abstract

Introduction

Conclusions

References

Tables

Figures

◀

▶

◀

▶

Back

Close

Full Screen / Esc

Printer-friendly Version

Interactive Discussion



9 Conclusions

A satellite remote sensing technology has been discussed, which has the potential to detect and monitor CO₂ emissions of moderate to strong localized CO₂ sources such as coal-fired power plants.

5 The instrument concept is based on an imaging spectrometer system which measures high spatial and high spectral resolution spectra of reflected solar radiation in the SWIR/NIR spectral region in nadir (and sun-glint) mode covering relevant absorption bands of CO₂, CH₄ and O₂. The instrument concept is similar as the concept developed for OCO and GOSAT but can serve additional important applications such as
10 power plant emission monitoring due to its wide swath imaging capability.

It has been shown that power plant CO₂ emissions can be unequivocally detected and quantified. The estimated CO₂ emission uncertainty is in the range 0.5–5 MtCO₂/year (1-sigma) for single power plant overpasses, which is about 2–20% of the emission of a large power plant. Using clear sky statistics it has been conservatively
15 estimated that about one useful measurement per 1–2 months can be obtained for a given power plant.

The investigated satellite system is however not limited to this application but will contribute to the detection and quantification of a number of other important localized CO₂ and CH₄ emission sources such as (mud) volcanoes.

20 The discussed satellite concept has the potential to become an important component of a future global CO₂ and CH₄ emission monitoring system, which is needed for example for independent verification of reported emissions in the context of Kyoto protocol follow-on agreements.

25 In addition to greenhouse gas emission hot spot detection, the satellite mission aims at fulfilling all relevant requirements for global regional-scale CO₂ and CH₄ surface flux inverse modelling, i.e., fulfills similar requirements as have been identified for OCO and GOSAT.

AMTD

3, 55–110, 2010

Monitoring CO₂ emissions from space

H. Bovensmann et al.

Title Page

Abstract

Introduction

Conclusions

References

Tables

Figures

◀

▶

◀

▶

Back

Close

Full Screen / Esc

Printer-friendly Version

Interactive Discussion



Monitoring CO₂ emissions from space

H. Bovensmann et al.

Title Page

Abstract

Introduction

Conclusions

References

Tables

Figures

◀

▶

◀

▶

Back

Close

Full Screen / Esc

Printer-friendly Version

Interactive Discussion



Assuming a launch in the 2014/15 time frame the satellite would continue the time series of global greenhouse gas (CO₂, CH₄) observations from space which started with the launch of ENVISAT with the SCIAMACHY instrument on board in 2002. This time series is currently being continued by the Japanese GOSAT satellite (launched in January 2009). At present however there are no firm plans to continue the SCIAMACHY/GOSAT CO₂ and CH₄ global time series. As a result there will likely be an observational gap in the time period 2014–2020. This gap can be closed with a satellite mission similar to the one investigated in this study. The presented concept assumes a single satellite but the spatio-temporal coverage could of course be significantly improved if the space based greenhouse gas monitoring system would consist of a constellation of greenhouse gas observing satellites.

Appendix A

Gaussian plume model

In order to simulate the CO₂ vertical column enhancement at and downwind of a CO₂ source such as a CO₂ emitting power plant, a quasi-stationary Gaussian plume model is used (Sutton, 1932). Integrated for the total vertical column V it equals:

$$V(x, y) = \frac{F}{\sqrt{2\pi}\sigma_y(x)u} e^{-\frac{1}{2}\left(\frac{y}{\sigma_y(x)}\right)^2}, \quad (\text{A1})$$

where V is the CO₂ vertical column (in g/m²) at and downwind of the point source. The x -direction is parallel to the wind direction and the y -direction perpendicular to the wind direction. V depends on the emission rate F (in g/s), the across wind distance y , wind speed u , and the standard deviation in y direction, σ_y . The standard deviation $\sigma_y = \sigma_y(x)$ is a function of the along wind distance x and depends on the atmospheric

stability parameter a (Masters, 1998, and references therein):

$$\sigma_y(x) = a \cdot x^{0.894}. \quad (\text{A2})$$

Here x must be specified in kilometers to give σ_y in meters. For stability class C (slightly unstable) Masters (1998) gives:

5 $a = 104. \quad (\text{A3})$

To simulate an emission source with a cross section y_0 at the plume's origin an offset x_0 is added to Eq. (A2):

$$\sigma_y(x) = a (x + x_0)^{0.894}, \quad (\text{A4})$$

where:

10 $x_0 = \left(\frac{y_0}{a}\right)^{\frac{1}{0.894}}. \quad (\text{A5})$

Appendix B

Retrieval algorithm BESD

15 Here we provide a description of the retrieval algorithm “Bremen optimal ESTimation DOAS” (BESD) as used for this study. BESD is based on Optimal Estimation (OE) (Rodgers, 2000) and on “Differential Optical Absorption Spectroscopy” (DOAS) (see, e.g., Buchwitz et al., 2000b, and references given therein). OE allows to constrain the retrieval using uncertain a-priori information, e.g., on aerosols and (thin) clouds. DOAS permits to filter out disturbing low frequency radiance contributions which are typically
20 difficult to model such as contributions from aerosol scattering, changes of the Earth's surface spectral reflectance and changes of instrument calibration functions. BESD is under development for improved SCIAMACHY CO₂ retrieval (Buchwitz et al., 2009; Reuter et al., 2009).

Title Page

Abstract

Introduction

Conclusions

References

Tables

Figures

◀

▶

◀

▶

Back

Close

Full Screen / Esc

Printer-friendly Version

Interactive Discussion



Monitoring CO₂ emissions from space

H. Bovensmann et al.

Title Page

Abstract

Introduction

Conclusions

References

Tables

Figures

◀

▶

◀

▶

Back

Close

Full Screen / Esc

Printer-friendly Version

Interactive Discussion



The satellite instrument measures radiance spectra $L_i \equiv L(\lambda_i)$ in nadir mode at discrete wavelengths λ_i as well as the solar irradiance, $F_i \equiv F(\lambda_i)$. For the following we assume that the wavelength grids of the nadir and the solar spectra are either identical or that the solar spectrum has been interpolated onto the wavelength grid of the nadir measurements. The directly measured quantities L_i and F_i are used to compute the measured sun-normalized radiance or intensity I_i which is defined as $I_i \equiv \pi R_i / F_i$. In the following the measurement vector \mathbf{y} is used whose elements are $y_i \equiv \ln(I_i)$. The corresponding model quantity \mathbf{y}^{mod} is obtained with the radiative transfer model (RTM) SCIATRAN (Buchwitz et al., 2000a; Rozanov et al., 2002). For this study we assume that the radiative transfer (RT) is sufficiently linear so that the logarithm of the sun-normalized radiance can be linearized around an assumed state of the (primarily) atmosphere denoted by the a-priori state vector \mathbf{x}_a . This is justified by the fact that the variations of the mixing ratios of the two well-mixed greenhouse gases investigated here, i.e., CO₂ and CH₄, are small. Therefore we assume that the following equation holds for \mathbf{y}^{mod} as a function of state vector \mathbf{x} :

$$\mathbf{y}^{\text{mod}}(\mathbf{x}) = \mathbf{y}_a + \mathbf{K}(\mathbf{x} - \mathbf{x}_a). \quad (\text{B1})$$

Here $\mathbf{y}_a \equiv \mathbf{y}^{\text{mod}}(\mathbf{x}_a)$, i.e., \mathbf{y}_a is the logarithm of the sun-normalized radiance for state vector \mathbf{x}_a . Matrix \mathbf{K} is the Jacobian matrix with elements $K_{ij} = f_j \partial y_i^{\text{mod}} / \partial x_j |_{\mathbf{x}=\mathbf{x}_a}$. For numerical reasons (most of) the elements of the Jacobian matrix are defined to be dimensionless. They express the relative change of the intensity due to a relative change of state vector element j (unit: %/%). For these cases $f_j = x_j$ and K_{ij} can be interpreted as the relative change of the intensity at wavelength λ_i due to a relative change of state vector element j . This is true for all state vector elements except for the elements which correspond to the coefficients of the low order polynomials. The low order polynomial is included to make the retrieval less sensitive to spectrally broadband radiance (and/or measured signal) contributions which typically cannot be modelled with high accuracy. For the polynomial coefficient x_j the corresponding elements of the Jacobian matrix are: $K_{ij} = ((\lambda_i - \lambda_c) / \lambda_c)^{n_p}$, where λ_c is the center wavelength of the

spectral fitting window for which the polynomial is valid. n_p is an integer in the range $0, \dots, N_p$, where N_p is the order of the polynomial (here we use a quadratic polynomial, i.e., $N_p=2$).

BESD is based on minimizing the following cost function $C(\mathbf{x})$:

$$C(\mathbf{x}) = (\mathbf{x} - \mathbf{x}_a)^T \mathbf{S}_{x_a}^{-1} (\mathbf{x} - \mathbf{x}_a) + (\mathbf{y} - \mathbf{y}^{\text{mod}}(\mathbf{x}))^T \mathbf{S}_y^{-1} (\mathbf{y} - \mathbf{y}^{\text{mod}}(\mathbf{x})). \quad (\text{B2})$$

Here \mathbf{x} is the to be estimated (atmospheric) state vector at the time of the measurement, \mathbf{x}_a is the assumed a-priori state vector (ideally the climatological mean) with a-priori variance/covariance matrix \mathbf{S}_{x_a} , \mathbf{y} is the measurement vector with variance/covariance matrix \mathbf{S}_y , and $\mathbf{y}^{\text{mod}}(\mathbf{x})$ is the forward model which relates the desired but unknown state vector with the directly measured quantity. Here $()^T$ denotes matrix transpose and $()^{-1}$ denotes matrix inverse.

The solution of this estimation problem is an estimate of the state vector, denoted $\hat{\mathbf{x}}$, and its variance/covariance matrix $\hat{\mathbf{S}}_x$. How this solution can be obtained is shortly described in the following (for details see (Rodgers, 2000; Rodgers and Connor, 2003) and references given therein).

Assuming Gaussian statistics and a linear forward model, which relates the state vector \mathbf{x} to the measured quantity \mathbf{y} via $\mathbf{y} = \mathbf{y}^{\text{mod}}(\mathbf{x}) + \epsilon$, where ϵ is the measurement error, the solution of this estimation problem, $\hat{\mathbf{x}}$, can be formulated in terms of the retrieval gain matrix \mathbf{G} :

$$\hat{\mathbf{x}} = \mathbf{x}_a + \mathbf{G}(\mathbf{y} - \mathbf{y}_a). \quad (\text{B3})$$

Gain matrix \mathbf{G} is defined as

$$\mathbf{G} = \frac{d\hat{\mathbf{x}}}{d\mathbf{y}} = \hat{\mathbf{S}}_x \mathbf{K}^T \mathbf{S}_y^{-1}. \quad (\text{B4})$$

Here $\hat{\mathbf{S}}_x$ is the uncertainty covariance matrix of $\hat{\mathbf{x}}$ and is given by

$$\hat{\mathbf{S}}_x = (\mathbf{K}^T \mathbf{S}_y^{-1} \mathbf{K} + \mathbf{S}_{x_a}^{-1})^{-1}. \quad (\text{B5})$$

Monitoring CO₂ emissions from space

H. Bovensmann et al.

Title Page

Abstract

Introduction

Conclusions

References

Tables

Figures

◀

▶

◀

▶

Back

Close

Full Screen / Esc

Printer-friendly Version

Interactive Discussion



An important matrix for the characterization of the retrieval is the averaging kernel matrix \mathbf{A} , which can be formulated in terms of \mathbf{G} and Jacobian matrix \mathbf{K} :

$$\mathbf{A} = \frac{d\hat{\mathbf{x}}}{d\mathbf{x}} = \frac{d\hat{\mathbf{x}}}{d\mathbf{y}} \frac{d\mathbf{y}}{d\mathbf{x}} = \mathbf{G}\mathbf{K}, \quad (\text{B6})$$

where \mathbf{x} is the true state vector (which is only exactly known for simulations).

The sum of the diagonal elements of \mathbf{A} is the so-called degree of freedom for signal $ds = \text{trace}(\mathbf{A})$, which can be interpreted as the number of “independent pieces of information” which can be retrieved.

Defining matrix $\mathbf{R} = \mathbf{A} - \mathbf{1}$, where $\mathbf{1}$ is a unit matrix, allows to compute another matrix, which is important for characterizing the retrieval, namely the smoothing error covariance matrix

$$\hat{\mathbf{S}}_s = \mathbf{R}\mathbf{S}_{x_a}\mathbf{R}^T, \quad (\text{B7})$$

which quantifies errors caused by limited (final) vertical resolution of the instrument. The measurement noise contribution to the overall uncertainty is given by the measurement noise covariance matrix

$$\hat{\mathbf{S}}_{y,x} = \mathbf{G}\mathbf{S}_y\mathbf{G}^T. \quad (\text{B8})$$

Of interest for this study are the absolute values of the state vector elements and the absolute values of functions of the state vector elements, in particular the total column of CO_2 and its statistical error. As the state vector \mathbf{x} has been defined using normalized dimensionless relative quantities, transformations from relative quantities to absolute quantities have to be carried out. The absolute value of state vector element j , \hat{x}_j^a , is related to its relative value, \hat{x}_j , by the following relation (here the alternative notation \bar{x} is used for the a-priori state vector, i.e., for \bar{x}_a , to avoid confusion with the the same letter a used for “a-priori” and “absolute”):

$$\hat{x}_j^a = \bar{x}_j^a(1 + \hat{x}_j). \quad (\text{B9})$$

Monitoring CO₂ emissions from space

H. Bovensmann et al.

Title Page

Abstract

Introduction

Conclusions

References

Tables

Figures

◀

▶

◀

▶

Back

Close

Full Screen / Esc

Printer-friendly Version

Interactive Discussion



This equation defines the transformation of the “relative state vector” $\hat{\mathbf{x}}$ to the corresponding “absolute state vector” $\hat{\mathbf{x}}^a$.

It can be shown that the state vector covariance matrix for the absolute state vector elements, $\hat{\mathbf{S}}_x^a$, can be obtained from the state vector covariance matrix for the relative state vector elements, $\hat{\mathbf{S}}_x$, as follows:

$$\left(\hat{\mathbf{S}}_x^a\right)_{ij} = \left(\bar{x}_i^a \bar{x}_j^a\right) \left(\hat{\mathbf{S}}_x\right)_{ij}. \quad (\text{B10})$$

Analogous relations exist for the smoothing error covariance matrix

$$\left(\hat{\mathbf{S}}_S^a\right)_{ij} = \left(\bar{x}_i^a \bar{x}_j^a\right) \left(\hat{\mathbf{S}}_S\right)_{ij} \quad (\text{B11})$$

and the measurement noise covariance matrix

$$\left(\hat{\mathbf{S}}_{yx}^a\right)_{ij} = \left(\bar{x}_i^a \bar{x}_j^a\right) \left(\hat{\mathbf{S}}_{yx}\right)_{ij}. \quad (\text{B12})$$

It can also be shown that the averaging kernel matrix for the absolute state vector elements can be obtained from the averaging kernel matrix for the relative state vector elements as follows:

$$\left(\mathbf{A}^a\right)_{ij} = \left(\mathbf{A}\right)_{ij} \frac{\bar{x}_i^a}{\bar{x}_j^a}. \quad (\text{B13})$$

The vertical column of, for example, CO₂, can be computed from the absolute state vector elements (i.e., layer columns), given above, and the total column operator \mathbf{g} , which can be defined as follows: $\mathbf{g}^T = [0, 0, 0, \dots, 1, 1, 1, \dots, 0, 0, 0]$, where $g_i = 1$ corresponds to state vector elements over which need to be summed to compute the total column (for CO₂ the indices of the state vector are $i = 0, 1$, and 2, as can be seen from Table 4). All other elements of \mathbf{g} , over which should not be summed, need to be set to 0. This formulation of \mathbf{g} requires that the corresponding CO₂ state vector elements are absolute sub-columns in, e.g., molecules/cm², as otherwise their sum will not yield the total vertical column.

Title Page

Abstract

Introduction

Conclusions

References

Tables

Figures

◀

▶

◀

▶

Back

Close

Full Screen / Esc

Printer-friendly Version

Interactive Discussion



Using these definitions, several important quantities, which are needed to characterize the retrieval, can be computed:

The a-priori vertical column of a gas of interest, e.g., CO₂, in absolute units (e.g., molecules/cm²) is given by

$$5 \quad \bar{v} = \mathbf{g}^T \bar{\mathbf{x}}^a. \quad (\text{B14})$$

The corresponding retrieved vertical column in absolute units is by

$$\hat{v} = \bar{v} + \mathbf{g}^T (\hat{\mathbf{x}}^a - \bar{\mathbf{x}}^a). \quad (\text{B15})$$

The corresponding vertical column total statistical error is

$$\sigma_v^2 = \mathbf{g}^T \hat{\mathbf{S}}_x^a \mathbf{g}. \quad (\text{B16})$$

10 The vertical column averaging kernel (a vector) is given by

$$\mathbf{a}_v^T = \mathbf{g}^T \mathbf{A}^a. \quad (\text{B17})$$

The vertical column smoothing error is

$$\sigma_{vs}^2 = \mathbf{g}^T \hat{\mathbf{S}}_s^a \mathbf{g} \quad (\text{B18})$$

and the vertical column measurement noise error is

$$15 \quad \sigma_{vyx}^2 = \mathbf{g}^T \hat{\mathbf{S}}_{yx}^a \mathbf{g}. \quad (\text{B19})$$

Finally, the dry air column-averaged mixing ratio of CO₂, denoted XCO₂, is computed from the retrieved CO₂ column (in molecules/cm²), denoted \hat{v}_{CO_2} , and the retrieved surface pressure (obtained from the retrieved pressure profile scaling factor), \hat{p}_o (in hPa). The retrieved XCO₂, denoted \hat{X}_{CO_2} (in ppm), is obtained as follows:

$$20 \quad \hat{X}_{\text{CO}_2} = \frac{\hat{v}_{\text{CO}_2}}{C \hat{p}_o / 1013.0}. \quad (\text{B20})$$

Title Page

Abstract

Introduction

Conclusions

References

Tables

Figures

◀

▶

◀

▶

Back

Close

Full Screen / Esc

Printer-friendly Version

Interactive Discussion



C is a constant and given by $C=10^{-6} \times 2.16 \times 10^{25}$. Factor 10^{-6} accounts for the conversion to ppm and 2.16×10^{25} is the assumed number of gaseous air molecules of dry air above a surface of area 1 cm^2 for a surface pressure of 1013 hPa.

The statistical uncertainty of the retrieved $X\text{CO}_2$ (in relative units), denoted $\sigma_{X\text{CO}_2}^r$, is computed from the relative statistical uncertainties of the retrieved CO_2 column and surface pressure:

$$\sigma_{X\text{CO}_2}^r = \sqrt{(\sigma_{\text{CO}_2} / \hat{\nu}_{\text{CO}_2})^2 + (\sigma_{p_s} / \hat{p}_s)^2}. \quad (\text{B21})$$

The statistical uncertainty of $X\text{CO}_2$ in absolute units (ppm) is given by (1-sigma):

$$\sigma_{X\text{CO}_2} = \sigma_{X\text{CO}_2}^r \times \hat{X}_{\text{CO}_2}. \quad (\text{B22})$$

Using analog formulas the corresponding result for methane, i.e., $\hat{X}_{\text{CH}_4} \pm \sigma_{X\text{CH}_4}$, can be obtained.

Acknowledgements. This study was funded by Wirtschaftsförderung Bremen (WFB) (Klima-Monitor project), DLR-Bonn (CarbonMon project), and ESA (ADVANSE project). We thank M. Wieser and C. Tobehn, OHB System AG, Bremen, for detailed CarbonSat orbit information and V. Mogulsky, B. Sang, and S. Hofer, Kayser-Threde GmbH, Munich, for CarbonSat instrument parameters. We thank NASA for the MODIS/Aqua data product (Collection 5, MYD35_L2 MODIS Level2 Cloud Mask data product obtained from <http://ladsweb.nascom.nasa.gov/data/search.html>). The spectral albedos have been obtained from the ASTER Spectral Library through courtesy of the Jet Propulsion Laboratory, California Institute of Technology, Pasadena, California (copyright 1999, California Institute of Technology) and the Digital Spectral Library 06 of the US Geological Survey. The general information about the power plants has been obtained from the CARMA data base (<http://carma.org>). We thank Dietmar Heinze, Vattenfall Europe Generation AG & Co. KG, Cottbus, Germany, for providing us with specific information on the actual emission of the power plant Schwarze Pumpe, Germany.

Title Page

Abstract

Introduction

Conclusions

References

Tables

Figures

◀

▶

◀

▶

Back

Close

Full Screen / Esc

Printer-friendly Version

Interactive Discussion



References

- Ackerman, S., Strabala, K., Menzel, W., Frey, R., Coeller, C., and Gumley, L.: Discriminating clear sky from clouds with MODIS, *J. Geophys. Res.*, 103, 32141–32157, 1998. 75
- Ackerman, S. A., Holz, R. E., Frey, R., Eloranta, E. W., Maddux, B. C., and McGill, M.: Cloud detection with MODIS. Part II: validation, *J. Atmos. Ocean. Tech.*, 25(7), 1073–1086, 2008. 75
- Amediek, A., Fix, A., Ehret, G., Caron, J., and Durand, Y.: Airborn lidar reflectance measurements at 1.57 μm in support of the A-SCOPE mission for atmospheric CO_2 , *Atmos. Meas. Tech.*, 2, 755–772, 2009, <http://www.atmos-meas-tech.net/2/755/2009/>. 60
- Aumann, H. H., Gregorich, D., and Gaiser, S.: AIRS hyper-spectral measurements for climate research: Carbon dioxide and nitrous oxide effects, *Geophys. Res. Lett.*, 32, L05806, doi:10.1029/2004GL021784, 2005. 60
- Baicu, C., Caracausi, A., Etiopie, G., and Italiano, F.: Mud volcanoes and methane seeps in Romania: main features and gas flux, *Ann. Geophys.*, 50(4), 501–511, 2007. 77
- Barkley, M. P., Frieß, U., and Monks, P. S.: Measuring atmospheric CO_2 from space using Full Spectral Initiation (FSI) WFM-DOAS, *Atmos. Chem. Phys.*, 6, 3517–3534, 2006a, <http://www.atmos-chem-phys.net/6/3517/2006/>. 59
- Barkley, M. P., Monks, P. S., and Engelen, R. J.: Comparison of SCIAMACHY and AIRS CO_2 measurements over North America during the summer and autumn of 2003, *Geophys. Res. Lett.*, 33, L20805, doi:10.1029/2006GL026807, 2006b. 59
- Barkley, M. P., Monks, P. S., Frieß, U., Mittermeier, R. L., Fast, H., Körner, S., and Heimann, M.: Comparisons between SCIAMACHY atmospheric CO_2 retrieved using (FSI) WFM-DOAS to ground based FTIR data and the TM3 chemistry transport model, *Atmos. Chem. Phys.*, 6, 4483–4498, 2006, <http://www.atmos-chem-phys.net/6/4483/2006/>. 59
- Barkley, M. P., Monks, P. S., Hewitt, A. J., Machida, T., Desai, A., Vinnichenko, N., Nakazawa, T., Yu Arshinov, M., Fedoseev, N., and Watai, T.: Assessing the near surface sensitivity of SCIAMACHY atmospheric CO_2 retrieved using (FSI) WFM-DOAS, *Atmos. Chem. Phys.*, 7, 3597–3619, 2007, <http://www.atmos-chem-phys.net/7/3597/2007/>. 59
- Bergamaschi, P., Frankenberg, C., Meirink, J. F., Krol, M., Dentener, F., Wagner, T., Platt, U.,

AMTD

3, 55–110, 2010

Monitoring CO_2 emissions from space

H. Bovensmann et al.

Title Page

Abstract

Introduction

Conclusions

References

Tables

Figures

◀

▶

◀

▶

Back

Close

Full Screen / Esc

Printer-friendly Version

Interactive Discussion



Kaplan, J. O., Körner, S., Heimann, M., Dlugokencky, E. J., and Goede, A.: Satellite cartography of atmospheric methane from SCIAMACHY onboard ENVISAT: 2. Evaluation based on inverse model simulations, *J. Geophys. Res.*, 112, D02304, doi:10.1029/2006JD007268, 2007. 59, 66

5 Bösch, H., Toon, G. C., Sen, B., Washenfelder, R. A., Wennberg, P. O., Buchwitz, M., de Beek, R., Burrows, J. P., Crisp, D., Christi, M., Connor, B. J., Natraj, V., and Yung, Y. L.: Space-based near-infrared CO₂ measurements: testing the orbiting carbon observatory retrieval algorithm and validation concept using SCIAMACHY observations over Park Falls, Wisconsin, *J. Geophys. Res.*, 111, D23302, doi:10.1029/2006JD007080, 2006. 59, 69

10 Bovensmann, H., Burrows, J. P., Buchwitz, M., Frerick, J., Noël, S., Rozanov, V. V., Chance, K. V., and Goede, A.: SCIAMACHY – mission objectives and measurement modes, *J. Atmos. Sci.*, 56, 127–150, 1999. 58

Buchwitz, M., Rozanov, V. V., and Burrows, J. P.: A correlated-k distribution scheme for overlapping gases suitable for retrieval of atmospheric constituents from moderate resolution radiance measurements in the visible/near-infrared spectral region, *J. Geophys. Res.*, 105, 15247–15262, 2000a. 59, 70, 81

15 Buchwitz, M., Rozanov, V. V., and Burrows, J. P.: A near infrared optimized DOAS method for the fast global retrieval of atmospheric CH₄, CO, CO₂, H₂O, and N₂O total column amounts from SCIAMACHY/ENVISAT-1 nadir radiances, *J. Geophys. Res.*, 105, 15231–15246, 2000b. 59, 63, 80

20 Buchwitz, M., de Beek, R., Burrows, J. P., Bovensmann, H., Warneke, T., Notholt, J., Meirink, J. F., Goede, A. P. H., Bergamaschi, P., Krner, S., Heimann, M., and Schulz, A.: Atmospheric methane and carbon dioxide from SCIAMACHY satellite data: initial comparison with chemistry and transport models, *Atmos. Chem. Phys.*, 5, 941–962, 2005, <http://www.atmos-chem-phys.net/5/941/2005/>. 59, 60

25 Buchwitz, M., de Beek, R., Noël, S., Burrows, J. P., Bovensmann, H., Bremer, H., Bergamaschi, P., Körner, S., and Heimann, M.: Carbon monoxide, methane and carbon dioxide columns retrieved from SCIAMACHY by WFM-DOAS: year 2003 initial data set, *Atmos. Chem. Phys.*, 5, 3313–3329, 2005, <http://www.atmos-chem-phys.net/5/3313/2005/>. 59

30 Buchwitz, M., de Beek, R., Noël, S., Burrows, J. P., Bovensmann, H., Schneising, O., Khlystova, I., Bruns, M., Bremer, H., Bergamaschi, P., Körner, S., and Heimann, M.: Atmospheric carbon gases retrieved from SCIAMACHY by WFM-DOAS: version 0.5 CO and

Monitoring CO₂ emissions from space

H. Bovensmann et al.

Title Page

Abstract

Introduction

Conclusions

References

Tables

Figures

◀

▶

◀

▶

Back

Close

Full Screen / Esc

Printer-friendly Version

Interactive Discussion



CH₄ and impact of calibration improvements on CO₂ retrieval, *Atmos. Chem. Phys.*, 6, 2727–2751, 2006,

<http://www.atmos-chem-phys.net/6/2727/2006/>. 59, 76, 77

Buchwitz, M., Schneising, O., Burrows, J. P., Bovensmann, H., Reuter, M., and Nothot, J.: First direct observation of the atmospheric CO₂ year-to-year increase from space, *Atmos. Chem. Phys.*, 7, 4249–4256, 2007 59

Buchwitz, M., Reuter, M., Schneising, O., Heymann, J., Bovensmann, H., and Burrows, J. P.: Towards an improved CO₂ retrieval algorithm for SCIAMACHY on ENVISAT, *Proceedings Atmospheric Science Conference, Barcelona, Spain, 7–11 Sept 2009, ESA Special Publication SP-676*, 2009. 60, 70, 80

Burrows, J. P., Hölzle, E., Goede, A. P. H., Visser H., and Fricke, W.: SCIAMACHY – scanning imaging absorption spectrometer for atmospheric cartography, *Acta Astronaut.*, 35(7), 445–451, 1995. 58

Burrows, J. P., Bovensmann, H., Bergametti, G., Flaud, J. M., Orphal, J., Noël, S., Monks, P. S., Corlett, G. K., Goede, A. P., von Clarmann, T., Steck, T., Fischer, H., and Friedl-Vallon, F.: The geostationary tropospheric pollution explorer (GeoTROPE) mission: objectives, requirements and mission concept, *Adv. Space Res.*, 34, 682–687, 2004. 60

Canadell, J. G., Le Quééré, C., Raupach, M. R., Field, C. B., Buitenhuis, E. T., Ciais, P., Conway, T. J., Gillett, N. P., Houghton, R. A., and Marland, G.: Contributions to accelerating atmospheric CO₂ growth from economic activity, carbon intensity, and efficiency of natural sinks, *Proceedings of the National Academy of Sciences (PNAS) of the United States of America*, November 20, 2007, 104, 18866–18870, 2007. 57

Chédin, A., Hollingsworth, A., Scott, N. A., Serrar, S., Crevoisier, C., and Armante, R.: Annual and seasonal variations of atmospheric CO₂, N₂O and CO concentrations retrieved from NOAA/TOVS satellite observations, *Geophys. Res. Lett.*, 29, 1269, doi:10.1029/2001GL014082, 2002. 60

Chédin, A., Serrar, S., Scott, N. A., Crevoisier, C., and Armante, R.: First global measurement of midtropospheric CO₂ from NOAA polar satellites: Tropical zone, *J. Geophys. Res.*, 108, 4581, doi:10.1029/2003JD003439, 2003. 60

Chevallier, F., Engelen, R. J., and Peylin, P.: The contribution of AIRS data to the estimation of CO₂ sources and sinks, *G. Res. Lett.*, 32, 23801, doi:10.1029/2005GL024229, 2005. 60

Chevallier, F., Bréon, F.-M., and Rayner, P. J.: Contribution of the orbiting carbon observatory to the estimation of CO₂ sources and sinks: theoretical study in a variational data assimilation

AMTD

3, 55–110, 2010

Monitoring CO₂ emissions from space

H. Bovensmann et al.

Title Page

Abstract

Introduction

Conclusions

References

Tables

Figures

◀

▶

◀

▶

Back

Close

Full Screen / Esc

Printer-friendly Version

Interactive Discussion



- framework, *J. Geophys. Res.*, 112, D09307, doi:10.1029/2006JD007375, 2007. 58, 64, 66
- Crevoisier, C., Chédin, A., Matsueda, H., Machida, T., Armante, R., and Scott, N. A.: First year of upper tropospheric integrated content of CO₂ from IASI hyperspectral infrared observations, *Atmos. Chem. Phys.*, 9, 4797–4810, 2009, <http://www.atmos-chem-phys.net/9/4797/2009/>. 60
- Crevoisier, C., Nobileau, D., Fiore, A. M., Armante, R., Chédin, A., Scott, N. A.: Tropospheric methane in the tropics – first year from IASI hyperspectral infrared observations, *Atmos. Chem. Phys.*, 9, 6337–6350, 2009, <http://www.atmos-chem-phys.net/9/6337/2009/>. 60
- Crisp, D., Atlas, R. M., Bréon, F.-M., Brown, L. R., Burrows, J. P., Ciais, P., Connor, B. J., Doney, S. C., Fung, I. Y., Jacob, D. J., Miller, C. E., O'Brien, D., Pawson, S., Randerson, J. T., Rayner, P., Salawitch, R. S., Sander, S. P., Sen, B., Stephens, G. L., Tans, P. P., Toon, G. C., Wennberg, P. O., Wofsy, S. C., Yung, Y. L., Kuang, Z., Chudasama, B., Sprague, G., Weiss, P., Pollock, R., Kenyon, D., and Schroll, S.: The Orbiting Carbon Observatory (OCO) mission, *Adv. Space Res.*, 34, 700–709, 2004. 58, 64, 65
- Crisp, D., Miller, C., Breon, F.M., Boesch, H., et al.: The Need for Atmospheric Carbon Dioxide Measurements from Space: Contributions from a Rapid Reflight of the Orbiting Carbon Observatory, http://www.nasa.gov/pdf/363474main_OCO_Reflight.pdf, p. 54, 12 May 2009.
- Christi, M. J. and Stephens, G. L.: Retrieving profiles of atmospheric CO₂ in clear sky and in the presence of thin cloud using spectroscopy from the near and thermal infrared: a preliminary case study, *J. Geophys. Res.*, 109, D04316, doi:10.1029/2003JD004058, 2004. 60
- Dimitrov, L.: Contribution to atmospheric methane by natural seepages on the Bulgarian continental shelf, *Cont. Shelf Res.*, 22, 2429–2442, 2002. 77
- Department of Energy and Environmental Protection Agency: Carbon Dioxide Emissions from the Generation of Electric Power in the United States, Washington, DC 20585 (DoE) and 20460 (EPA), July 2000, p. 19, 2000. 57
- Engelen, R. J. and Stephens, G. L.: Information content of infrared satellite sounding measurements with respect to CO₂, *J. Appl. Meteorol.*, 43, 373–378, 2004, 60
- Engelen, R. J., Andersson, E., Chevallier, F., Hollingsworth, A., Matricardi, M., McNally, A. P., Thépaut, J.-N., and Watts, P. D.: Estimating atmospheric CO₂ from advanced infrared satellite radiances within an operational 4-D-Var data assimilation system: Methodology and first results, *J. Geophys. Res.*, 109, D19309, doi:10.1029/2004JD004777, 2004. 60
- Engelen, R. J. and McNally, A. P.: Estimating atmospheric CO₂ from advanced infrared satellite

Monitoring CO₂ emissions from spaceH. Bovensmann et al.

[Title Page](#)[Abstract](#)[Introduction](#)[Conclusions](#)[References](#)[Tables](#)[Figures](#)[◀](#)[▶](#)[◀](#)[▶](#)[Back](#)[Close](#)[Full Screen / Esc](#)[Printer-friendly Version](#)[Interactive Discussion](#)

- radiances within an operational 4-D-Var data assimilation system: Results and validation, *J. Geophys. Res.*, 109, D18305, doi:10.1029/2005JD005982, 2005. 60
- Etiopie, G.: Natural emissions of methane from geological seepage in Europe, *Atmos. Environ.*, 43, doi:10.1016/j.atmosenv.2008.03.014, 1430–1443, 2009. 77
- 5 Etiopie, G., Feyzullayev, A., and Baicu, C. L.: Terrestrial methane seeps and mud volcanoes: a global perspective of gas origin, *Mar. Petrol. Geol.*, 26, doi:10.1016/j.marpetgeo.2008.03.001, 333–344, 2009. 77
- Frankenberg, C., Meirink, J. F., van Weele, M., Platt, U., and Wagner, T.: Assessing methane emissions from global spaceborne observations, *Science*, 308, 1010–1014, 2005. 59, 76
- 10 Frankenberg, C., Bergamaschi, P., Butz, A., Houweling, S., Meirink, J. F., Notholt, J., Petersen, A. K., Schrijver, H., Warneke, T., and Aben, I.: Tropical methane emissions: a revised view from SCIAMACHY onboard ENVISAT, *Geophys. Res. Lett.*, 35, L15811, doi:10.1029/2008GL034300, 2008. 59, 76, 77
- Frey, R. A., Ackerman, S. A., Liu, Y. H., Strabala, K. I., Zhang, H., Key, J. R., and Wang, X. G.: Cloud detection with MODIS. Part I: improvements in the MODIS cloud mask for collection 5, *J. Atmos. Ocean. Tech.*, 25(7), 1057–1072, 2008. 75
- Gerilowski, K., Tretner, A., Krings, T., Buchwitz, M., Bertagnolio, P. P., Belemezov, F., Erzinger, J., Burrows, J. P., and Bovensmann, H.: MAMAP – A new spectrometer system for column-averaged methane and carbon dioxide observations from aircraft: Instrument description and initial performance assessment, in preparation, 2010.
- 20 Gloudemans, A. M. S., Schrijver, H., Kleipool, Q., van den Broek, M. M. P., Straume, A. G., Lichtenberg, G., van Hees, R. M., Aben, I., and Meirink, J. F.: The impact of SCIAMACHY near-infrared instrument calibration on CH₄ and CO total columns, *Atmos. Chem. Phys.*, 5, 2369–2383, 2005, <http://www.atmos-chem-phys.net/5/2369/2005/>. 59
- 25 Greig, J. S., Andres, R. J., and Marland, G.: China: emissions pattern of the world leader in CO₂ emissions from fossil fuel consumptions and cement production, *Geophys. Res. Lett.*, 35, L08806, doi:10.1029/2007GJ032887, 1–5, 2008. 58
- Hamazaki, T., Kaneko, Y., and Kuze, A.: Carbon dioxide monitoring from the GOSAT satellite, Proceedings XXth ISPRS conference, Istanbul, Turkey, 12–23 July 2004, p. 3, <http://www.isprs.org/congresses/istanbul2004/comm7/papers/43.pdf>, 2004. 58, 65
- 30 Houweling, S., Breon, F.-M., Aben, I., Rödenbeck, C., Gloor, M., Heimann, M., and Ciais, P.: Inverse modeling of CO₂ sources and sinks using satellite data: a synthetic inter-comparison

Monitoring CO₂ emissions from spaceH. Bovensmann et al.

Title Page

Abstract

Introduction

Conclusions

References

Tables

Figures

◀

▶

◀

▶

Back

Close

Full Screen / Esc

Printer-friendly Version

Interactive Discussion



- of measurement techniques and their performance as a function of space and time, *Atmos. Chem. Phys.*, 4, 523–538, 2004,
<http://www.atmos-chem-phys.net/4/523/2004/>. 58, 64, 66
- Houweling, S., Hartmann, W., Aben, I., Schrijver, H., Skidmore, J., Roelofs, G.-J., and Breon, F.-M.: Evidence of systematic errors in SCIAMACHY-observed CO₂ due to aerosols, *Atmos. Chem. Phys.*, 5, 3003–3013, 2005,
<http://www.atmos-chem-phys.net/5/3003/2005/>. 59
- Solomon, S., Qin, D., Manning, M., Chen, Z., Marquis, M., Averyt, K. B., Tignor, M., and Miller, H. L. (eds.): *Climate Change 2007: The Physical Science Basis*, Contribution of Working Group I to the Fourth Assessment Report of the Intergovernmental Panel on Climate Change (IPCC), Cambridge University Press, 996 pp., 2007. 57
- Jagovkina, S. V., Karol, I. L., Zubov, V. A., Lagun, V. E., Reshetnikov, A. I., and Rozanov, E. V.: Reconstruction of the methane fluxes from the West Siberian gas fields by the 3-D regional chemical tranprt model, *Atmos. Environ.*, 34, 5319–5329, 2000. 77
- Kourtidis, K., Kioutsioukis, I., McGinnis, D. F., and Rapsomanikis, S.: Effects of methane outgassing on the Black Sea atmosphere, *Atmos. Chem. Phys.*, 6, 5173–5182, 2006,
<http://www.atmos-chem-phys.net/6/5173/2006/>. 77
- Krings, T., Buchwitz, M., Gerilowski, K., et al.: MAMAP – A new spectrometer system for column-averaged methane and carbon dioxide observations from aircraft: Retrieval algorithm and first inversions for point source emission rates, in preparation, 2010.
- Kuang, Z., Margolis, J., Toon, G., Crisp, D., and Yung, Y.: Spaceborne measurements of atmospheric CO₂ by high-resolution NIR spectrometry of reflected sunlight: an introductory study, *Geophys. Res. Lett.*, 29, 1716, doi:10.1029/2001GL014298, 2002. 58, 72
- Leifer, I., Roberts, D., Margolis, J., and Kinnaman, F.: In situ sensing of methane emissions from natural marine hydrocarbon seeps: A potential remote sensing technology, *Earth Planet. Sc. Lett.*, 245, 509–522, 2006a. 77
- Leifer, I., Luyendyk, B. P., Boles, J., and Clark, J. F.: Natural methane seepage blowout: contribution to atmospheric methane, *Global Biogeochem. Cy.*, 20, GB3008, doi:10.1029/2005GB002668, 1–9, 2006b. 77
- Leliveld, J., Lechtenböhmer, S., Assonov, S. S., Brenninkmeijer, C. A. M., Dienst, C., Fishedick, M., and Hanke, T.: Low methane leakage from gas pipelines, *Nature*, 434, 841–842, 2005. 77
- Masters, G. M.: *Introduction to Environmental Engineering and Science*, Prentice-Hall, Inc.,

**Monitoring CO₂
emissions from
space**H. Bovensmann et al.

[Title Page](#)[Abstract](#)[Introduction](#)[Conclusions](#)[References](#)[Tables](#)[Figures](#)[◀](#)[▶](#)[◀](#)[▶](#)[Back](#)[Close](#)[Full Screen / Esc](#)[Printer-friendly Version](#)[Interactive Discussion](#)

2nd edn., 413 pp., 1998. 80

Meirink, J. F., Eskes, H. J., and Goede, A. P. H.: Sensitivity analysis of methane emissions derived from SCIAMACHY observations through inverse modelling, *Atmos. Chem. Phys.*, 6, 1275–1292, 2006,

<http://www.atmos-chem-phys.net/6/1275/2006/>. 59, 66

Meirink, J. F., Bergamaschi, P., and Krol, M. C.: Four-dimensional variational data assimilation for inverse modelling of atmospheric methane emissions: method and comparison with synthesis inversion, *Atmos. Chem. Phys.*, 8, 6341–6353, 2008,

<http://www.atmos-chem-phys.net/8/6341/2008/>. 59

Miller, C. E., Crisp, D., DeCola, P. L., Olsen, S. C., Randerson, J. T., Michalak, A. M., Alkhaled, A., Rayner, P., Jacob, D. J., Suntharalingam, P., Jones, D. B. A., Denning, A. S., Nicholls, M. E., Doney, S. C., Pawson, S., Boesch, H., Connor, B. J., Fung, I. Y., O'Brien, D. O., Salawitch, R. J., Sander, S. P., Sen, B., Tans, P., Toon, G. C., Wennberg, P. O., Wofsy, S. C., Yung, Y. L., and Law, R. M.: Precision requirements for space-based X_{CO_2} data, *J. Geophys. Res.*, 112, D10314, doi:10.1029/2006JD007659, 2007. 58, 64, 66

Palmer, P. I. and Rayner, P.: Atmospheric science: failure to launch, *Nature Geosci.*, 2, 247, doi:10.1038/ngeo495, 2009. 58

Rayner, P. J. and O'Brien, D. M.: The utility of remotely sensed CO_2 concentration data in surface inversions, *Geophys. Res. Lett.*, 28, 175–178, 2001. 58

Rehder, G., Keir, R. S., Suess, E., and Pohlmann, T.: The multiple sources and patterns of methane in North Sea water, *Aquat. Geochem.*, 4, 403–427, 1998. 77

Reuter, M., Buchwitz, M., Schneising, O., Heymann, J., Bovensmann, H., and Burrows, J. P.: A method for improved SCIAMACHY CO_2 retrieval in the presence of optically thin clouds, *Atmos. Meas. Tech. Discuss.*, 2, 2483–2538, 2009,

<http://www.atmos-meas-tech-discuss.net/2/2483/2009/>. 60, 70, 80

Rodgers, C. D.: *Inverse Methods for Atmospheric Sounding: Theory and Practice*, World Scientific Publishing, 2000. 70, 80, 82

Rodgers, C. D. and Connor, B. J.: Intercomparison of remote sounding instruments, *J. Geophys. Res.*, 108(D3), 2003. 82

Rozanov, V. V., Buchwitz, M., Eichmann, K.-U., de Beek, R., and Burrows, J. P.: SCIATRAN – a new radiative transfer model for geophysical applications in the 240–2400 nm spectral region: the pseudo-spherical version, *Adv. Space Res.*, 29, 1831–1835, 2002. 70, 81

Schneising, O., Buchwitz, M., Burrows, J. P., Bovensmann, H., Reuter, M., Notholt, J., Macatan-

Monitoring CO_2 emissions from space

H. Bovensmann et al.

Title Page

Abstract

Introduction

Conclusions

References

Tables

Figures

◀

▶

◀

▶

Back

Close

Full Screen / Esc

Printer-friendly Version

Interactive Discussion



gay, R., and Warneke, T.: Three years of greenhouse gas column-averaged dry air mole fractions retrieved from satellite – Part 1: Carbon dioxide, *Atmos. Chem. Phys.*, 8, 3827–3853, 2008,

<http://www.atmos-chem-phys.net/8/3827/2008/>. 59, 60, 72

5 Schneising, O., Buchwitz, M., Burrows, J. P., Bovensmann, H., Bergamaschi, P., and Peters, W.: Three years of greenhouse gas column-averaged dry air mole fractions retrieved from satellite – Part 2: Methane, *Atmos. Chem. Phys.*, 9, 443–465, 2009,

<http://www.atmos-chem-phys.net/9/443/2009/>. 59, 72, 76, 77

Shindell, D. T. and Faluvegi, G.: The net climate impact of coal-fired power plant emissions, *Atmos. Chem. Phys. Discuss.*, 9, 21257–21284, 2009,

10 <http://www.atmos-chem-phys-discuss.net/9/21257/2009/>. 57

Shakhova, N. E., Sergienko, V. I., and Semiletov, I. P.: The contribution of the East Siberian Shelf to the Modern Methane Cycle, *Herald of the Russian Academy of Sciences*, ISSN 1019–3316, Vol. 79, No. 3, 237–246, 2009. 61, 77

15 Solomon, E. A., Kastner, M., MacDonald, I. R., and Leifer, I.: Considerable methane fluxes to the atmosphere from hydrocarbon seeps in the Gulf of Mexico, *Nature Geosci.*, 2, doi:10.1038/NGEO574, 561–563, 2009. 77

Spinetti, C., Carrère, V., Buongiorno, M. F., Sutton, A. J., and Elias, T.: Carbon dioxide of Pu'u'O'o volcanic plume at Kilauea retrieved by AVIRS hyperspectral data, *Remote Sens. Environ.*, 112, doi:10.1016/j.rse.2008.03.010, 3192–3199, 2008. 77

20 Strow, L. L., Hannon, S. E., De-Souza Machado, S., Motteler, H. E., and Tobin, D. C.: Validation of the atmospheric infrared sounder radiative transfer algorithm, *J. Geophys. Res.*, 111, D09S06, doi:10.1029/2005JD006146, 2006. 60

Sutton, O. G.: A Theory of Eddy Diffusion in the Atmosphere, *Proceedings of the Royal Society of London, Series A, Containing Papers of a Mathematical and Physical Character*, The Royal Society of London, London, UK, 135(826), 143–165, 1932. 79

25 Westbrook, G. K., Thatcher, K. E., Rohling, E. J. et al.: Escape of methane from the seabed along West Spitsbergen continental margin, *Geophys. Res. Lett.*, 36, L15608, doi:10.1029/2009GL039191, 2009. 61, 77

AMTD

3, 55–110, 2010

Monitoring CO₂ emissions from space

H. Bovensmann et al.

Title Page

Abstract

Introduction

Conclusions

References

Tables

Figures

◀

▶

◀

▶

Back

Close

Full Screen / Esc

Printer-friendly Version

Interactive Discussion



Monitoring CO₂ emissions from space

H. Bovensmann et al.

Table 1. Maximum CO₂ column enhancement (relative to the background column (=1.0)) for a power plant emitting 13 Mt CO₂/year for different spatial resolutions of the satellite footprint. The assumed wind speed is 1 m/s.

Resolution	Peak of CO ₂ column relative to background (–)	Remark
20 m×20 m	1.126	see Fig. 1 left
40 m×40 m	1.125	
1 km×1 km	1.053	see Fig. 1 right
2 km×2 km	1.031	
4 km×4 km	1.017	
10 km×10 km	1.005	

Title Page

Abstract

Introduction

Conclusions

References

Tables

Figures

⏪

⏩

◀

▶

Back

Close

Full Screen / Esc

Printer-friendly Version

Interactive Discussion



Monitoring CO₂ emissions from space

H. Bovensmann et al.

Table 2. CarbonSat’s spectral bands, assumed performance parameters and corresponding signal-to-noise ratios (SNRs). Each band is equipped with a Focal Plane Array (FPA) with approx 1000×250 detector pixels in the spectral and spatial directions, respectively. The spectral resolution is specified in terms of the Full Width at Half Maximum (FWHM) of the spectrometer’s line shape function. The spectral sampling ratio is the number of detector pixels per FWHM. The SNR refers to the continuum SNR outside strong absorption lines for nadir measurements with an integration time of $t_{\text{int}}=0.25$ s and for a ground pixel size of 4 km². The assumed orbit altitude is 800 km. The SNRs are given for the 9 scenarios specified in Table 3.

Parameter	NIR	Band SWIR-1	SWIR-2
Spectral range (nm)	757–775	1559–1675	2043–2095
Spectral resolution FWHM (nm)	0.045	0.34	0.123
Spectral sampling ratio N_{sr} (1/nm)	3	3	3
Transmission T (–)	0.5	0.5	0.5
Quantum efficiency QE (electrons/photon)	0.6	0.6	0.6
Detector area A_{det} (10 ^{–6} cm ²)	5.76	5.76	5.76
F -number F_{num} (–)	2.0	2.0	2.0
Detector dark current I_{dark} (fA)	0.1	3.0	3.0
Thermal background current I_{back} (fA)	0.0	0.0	2.0
Readout noise N_{read} (electrons r.m.s.)	6	300	300
Continuum SNR (–):			
VEG_25: Vegetation, SZA=25°	390	400	70
SAS_25: Sand/soil, SZA=25°	390	750	250
VEG_50: Vegetation, SZA=50°	330	330	55
SAS_50: Sand/soil, SZA=50°	330	600	190
A01_50: Albedo=0.1, SZA=50°	220	330	90
A005_60: Albedo=0.05, SZA=60°	220	220	50
VEG_75: Vegetation, SZA=75°	235	210	35
SAS_75: Sand/soil, SZA=75°	235	360	90
WAT_75: Worst case	180	140	30

Title Page

Abstract

Introduction

Conclusions

References

Tables

Figures

◀

▶

◀

▶

Back

Close

Full Screen / Esc

Printer-friendly Version

Interactive Discussion



Monitoring CO₂ emissions from space

H. Bovensmann et al.

Table 3. Specification of 9 scenarios and corresponding retrieval precisions for CO₂ and CH₄ columns, surface pressure, and XCO₂.

Scenario	Albedo (–) NIR/SWIR-1/SWIR-2	SZA (deg.)	CO ₂ col. (%)	Retrieval precision		
				Surf. press. (%)	CH ₄ col. (%)	XCO ₂ (ppm)
VEG_25: Vegetation, SZA=25°	0.2/0.1/0.05	25	0.26	0.11	0.42	1.1
SAS_25: Sand/soil, SZA=25°	0.2/0.3/0.3	25	0.15	0.10	0.22	0.7
VEG_50: Vegetation, SZA=50°	0.2/0.1/0.05	50	0.28	0.08	0.47	1.2
SAS_50: Sand/soil, SZA=50°	0.2/0.3/0.3	50	0.16	0.08	0.24	0.7
A01_50: Albedo=0.1, SZA=50°	0.1/0.1/0.1	50	0.25	0.13	0.46	1.1
A005_60: Albedo=0.05, SZA=60°	0.05/0.05/0.05	60	0.48	0.22	0.83	2.1
VEG_75: Vegetation, SZA=75°	0.2/0.1/0.05	75	0.37	0.38	0.72	2.1
SAS_75: Sand/soil, SZA=75°	0.2/0.3/0.3	75	0.26	0.26	0.36	1.5
WAT_75: Worst case	0.02/0.02/0.02	75	0.84	0.44	1.61	3.7

[Title Page](#)
[Abstract](#)
[Introduction](#)
[Conclusions](#)
[References](#)
[Tables](#)
[Figures](#)
[Back](#)
[Close](#)
[Full Screen / Esc](#)
[Printer-friendly Version](#)
[Interactive Discussion](#)


Monitoring CO₂ emissions from space

H. Bovensmann et al.

Table 4. BESD retrieval algorithm state vector elements and a-priori uncertainties. PSU is the surface pressure state vector element with corresponding 1-sigma uncertainty of 3%. The nine POL parameters are the coefficients of the quadratic polynomials in the three spectral bands. ACS are the three state vector elements for aerosol and cloud scattering in the three atmospheric layers stratosphere (ST), upper troposphere (UT) and lower troposphere (LT). In the three bottom rows the CO₂ state vector elements are listed, which are layer columns). The assumed 1-sigma uncertainty of the CO₂ lower tropospheric layer column (ID CO2_00) is 6%. Tighter constraints are used for CO₂ in the upper layers. For CH₄ the constraints are relaxed as methane is assumed to be more variable compared to CO₂. For H₂O and temperature single vertical profile scaling factors have been defined as state vector elements.

Number	ID	Explanation	Uncertainty (relative) (-)
20	PSU.00	Surface pressure	0.030
		Polynom NIR	
19	POLa02	Quadratic term	1000.0
18	POLa01	Linear term	1000.0
17	POLa00	Constant term	1000.0
		Polynom SWIR-1	
16	POLb02	Quadratic term	1000.0
15	POLb01	Linear term	1000.0
14	POLb00	Constant term	1000.0
		Polynom SWIR-2	
13	POLc02	Quadratic term	1000.0
12	POLc01	Linear term	1000.0
11	POLc00	Constant term	1000.0
10	ACS.02	Aero./clouds scat. ST	0.050
9	ACS.01	Aero./clouds scat. UT	5.000
8	ACS.00	Aero./clouds scat. LT	1.000
7	H2O.00	H ₂ O(z) scaling	2.000
6	TEM.00	T(z) scaling	0.100
5	CH4.02	CH ₄ ST	0.010
4	CH4.01	CH ₄ UT	0.060
3	CH4.00	CH ₄ LT	0.120
2	CO2.02	CO ₂ ST	0.005
1	CO2.01	CO ₂ UT	0.030
0	CO2.00	CO ₂ LT	0.060

[Title Page](#)
[Abstract](#)
[Introduction](#)
[Conclusions](#)
[References](#)
[Tables](#)
[Figures](#)
[Back](#)
[Close](#)
[Full Screen / Esc](#)
[Printer-friendly Version](#)
[Interactive Discussion](#)


Monitoring CO₂ emissions from space

H. Bovensmann et al.

Title Page

Abstract

Introduction

Conclusions

References

Tables

Figures

◀

▶

◀

▶

Back

Close

Full Screen / Esc

Printer-friendly Version

Interactive Discussion



Table 5. Uncertainty of retrieved power plant CO₂ emissions (1-sigma) for three different XCO₂ single measurement precisions, two different power plant CO₂ emissions, and three wind speeds.

XCO ₂ retrieval uncertainty (ppm)	Power plant emission (Mt CO ₂ /year)	Wind speed (m/s)	Uncertainty of retrieved CO ₂ emission (Mt CO ₂ /year)
1 ppm (0.25%)	6.5	1	0.42
1 ppm (0.25%)	6.5	2	0.85
1 ppm (0.25%)	6.5	4	2.32
1 ppm (0.25%)	13.0	1	0.42
1 ppm (0.25%)	13.0	2	0.83
1 ppm (0.25%)	13.0	4	1.70
2 ppm (0.5%)	6.5	1	0.84
2 ppm (0.5%)	6.5	2	1.71
2 ppm (0.5%)	6.5	4	4.65
2 ppm (0.5%)	13.0	1	0.85
2 ppm (0.5%)	13.0	2	1.68
2 ppm (0.5%)	13.0	4	3.43
4 ppm (1.0%)	6.5	1	1.68
4 ppm (1.0%)	6.5	2	3.43
4 ppm (1.0%)	6.5	4	9.30
4 ppm (1.0%)	13.0	1	1.69
4 ppm (1.0%)	13.0	2	3.36
4 ppm (1.0%)	13.0	4	6.85

Monitoring CO₂ emissions from space

H. Bovensmann et al.

Table 6. Clear sky probabilities for CarbonSat overpasses over different selected power plants, ordered by latitude, for one entire year and for the four seasons December–February (DJF) to September–October (SON), derived from the MODIS/Aqua 2008 cloud mask data product. The clear sky probabilities are valid for 16 km×16 km large scenes. The power plant names, locations and emissions have been obtained from the CARMA data base (<http://carma.org>).

Power plant name	Country	CO ₂ emission (MtCO ₂ /year)	Latitude (deg)	Longitude (deg)	Clear sky probability				
					Entire year (%)	DJF (%)	MAM (%)	JJA (%)	SON (%)
REFTINSKAYA SDPP	Russia	22.2	57.1	61.6	7.0	1.6	8.3	12.4	5.7
DRAX	UK	22.6	53.7	−1.0	6.8	15.9	4.7	1.9	4.9
JANSCHWALDE	Germany	27.4	51.8	14.4	8.7	8.5	9.2	8.2	8.7
SCHWARZE PUMPE	Germany	11.9	51.5	14.3	8.7	8.5	9.2	8.2	8.7
BELCHATOW	Poland	34.6	51.3	19.3	10.0	7.6	6.8	14.8	10.8
NIEDERAUSSEM	Germany	30.4	51.0	6.7	8.7	14.3	8.4	7.5	4.5
TUOKETUO-1	China	24.7	40.8	111.8	23.6	9.2	20.6	23.7	40.5
GIBSON	USA	22.4	40.5	−88.3	17.4	8.1	18.1	15.4	27.6
NAVAJO	USA	19.1	36.9	−111.4	34.9	9.5	34.6	35.1	59.7
TANGJIN	South Korea	24.7	36.9	126.6	17.3	17.8	26.1	8.8	16.7
ZOUXIAN	China	34.5	36.4	116.0	25.2	19.7	34.5	11.5	34.8
OROT RABIN	Israel	21.2	32.4	34.9	35.1	24.8	35.8	41.0	38.5
WA PARISH	USA	20.9	29.5	−95.6	20.5	19.3	24.6	2.2	36.0
VINDHYACHAL	India	20.2	24.4	81.9	38.1	73.5	38.8	0.0	41.5
TAISHAN	China	19.6	22.2	112.8	14.1	32.6	5.4	0.3	19.2
PETACALCO	Mexico	19.3	21.2	−99.0	19.7	34.3	29.9	1.8	13.0
TALCHER STPS	India	23.4	20.8	85.1	25.4	58.8	23.4	0.1	20.9
RAMAGUNDAM	India	21.4	18.4	79.2	32.1	69.1	30.6	0.0	28.7
MAE MOH	Thailand	21.7	18.3	99.7	10.4	29.9	4.4	0.0	7.6
NEYVELI	India	20.5	11.5	79.5	11.4	20.6	14.9	0.8	9.5
SURALAYA	Indonesia	25.8	−6.1	106.1	2.8	0.2	1.2	8.9	1.1
KENDAL	South Africa	26.8	−30.1	27.1	31.6	13.3	18.1	51.9	42.6
BAYSWATER	Australia	19.8	−32.3	150.9	22.0	10.7	28.9	26.5	21.2
ERARING	Australia	19.8	−33.1	151.5	27.4	17.8	35.6	29.1	26.6
Average:					19.1	21.9	19.7	12.9	22.0

Title Page

Abstract

Introduction

Conclusions

References

Tables

Figures

◀

▶

◀

▶

Back

Close

Full Screen / Esc

Printer-friendly Version

Interactive Discussion



Monitoring CO₂ emissions from space

H. Bovensmann et al.

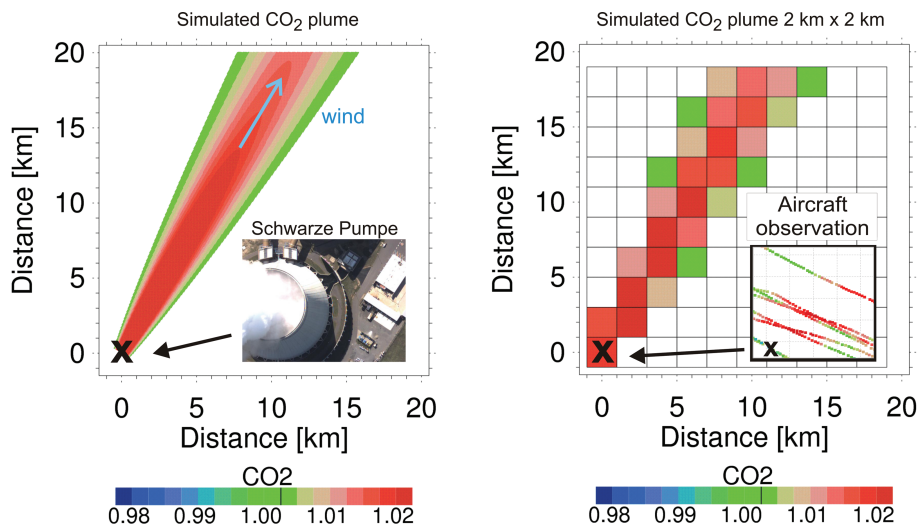


Fig. 1. Left: Simulation of the atmospheric CO₂ column enhancement due to CO₂ emission of a power plant using a quasi-stationary Gaussian plume model. The power plant location is indicated by the black cross. A value of 1.0 (green) corresponds to the background CO₂ column. A value of 1.02 (red) corresponds to a column enhancement of 2% or larger relative to the background. The wind speed is 1 m/s. The assumed power plant emission is 13 MtCO₂/year corresponding to a power plant such as Schwarze Pumpe located in eastern Germany near Berlin (see photo taken during an overflight with the MAMAP/CarbonMapper aircraft instrument). Right: as left hand side but at a spatial resolution of 2×2 km² obtained by box-car averaging the high resolution plume shown on the left hand side. The inset shows MAMAP/CarbonMapper CO₂ column retrievals around the location of the power plant Schwarze Pumpe (see main text and Fig. 2 for details). The maximum value of the CO₂ normalized column is 1.126 for the high resolution plume on the left (resolution 20×20 m²) and 1.031 for the 2×2 km² resolution plume shown on the right. To better visualize the extent of the CO₂ plumes values below 1.0025 are shown in white (see also the black vertical line in the color bar).

Title Page

Abstract

Introduction

Conclusions

References

Tables

Figures

◀

▶

◀

▶

Back

Close

Full Screen / Esc

Printer-friendly Version

Interactive Discussion



Monitoring CO₂ emissions from space

H. Bovensmann et al.

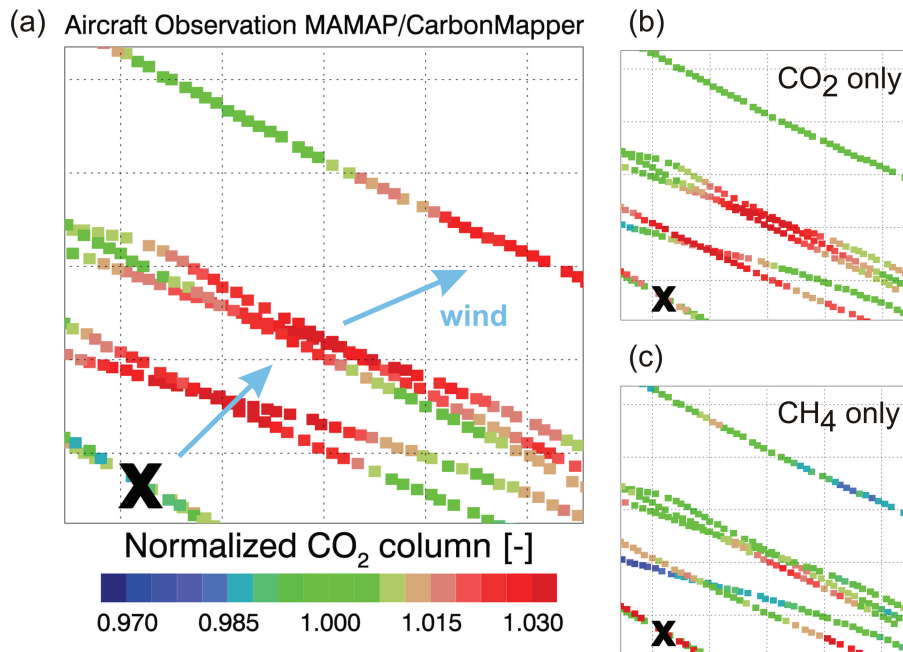


Fig. 2. (a) Normalized CO₂ columns as retrieved from MAMAP/CarbonMapper aircraft observations on 26 July 2007. The CO₂ columns have been normalized by simultaneously retrieved CH₄ columns. (b) Retrieved CO₂ columns without normalization by CH₄. (c) Retrieved CH₄ columns. The black cross indicates the location of the power plant Schwarze Pumpe (latitude 51.54° N, longitude 14.35° E), Germany. The blue arrows indicate the approximate wind direction, which changed during the time of the measurements.

[Title Page](#)[Abstract](#)[Introduction](#)[Conclusions](#)[References](#)[Tables](#)[Figures](#)[◀](#)[▶](#)[◀](#)[▶](#)[Back](#)[Close](#)[Full Screen / Esc](#)[Printer-friendly Version](#)[Interactive Discussion](#)

**Monitoring CO₂
emissions from
space**

H. Bovensmann et al.

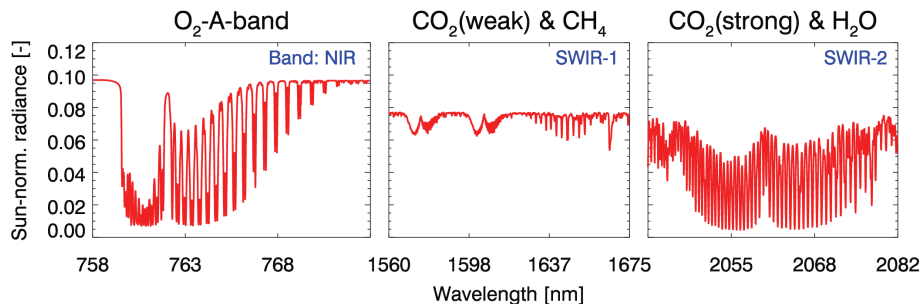


Fig. 3. Simulated CarbonSat spectra of the sun-normalized radiance for nadir observation of a scene with surface albedo 0.1 and solar zenith angle of 50°. Shown are the three spectrometer bands covered by CarbonSat: Left: O₂-A-band spectral region (“NIR” band), middle: weak CO₂ and CH₄ band region (“SWIR-1”), right: strong CO₂ band region (“SWIR-2”).

[Title Page](#)[Abstract](#)[Introduction](#)[Conclusions](#)[References](#)[Tables](#)[Figures](#)[◀](#)[▶](#)[◀](#)[▶](#)[Back](#)[Close](#)[Full Screen / Esc](#)[Printer-friendly Version](#)[Interactive Discussion](#)

Monitoring CO₂ emissions from space

H. Bovensmann et al.

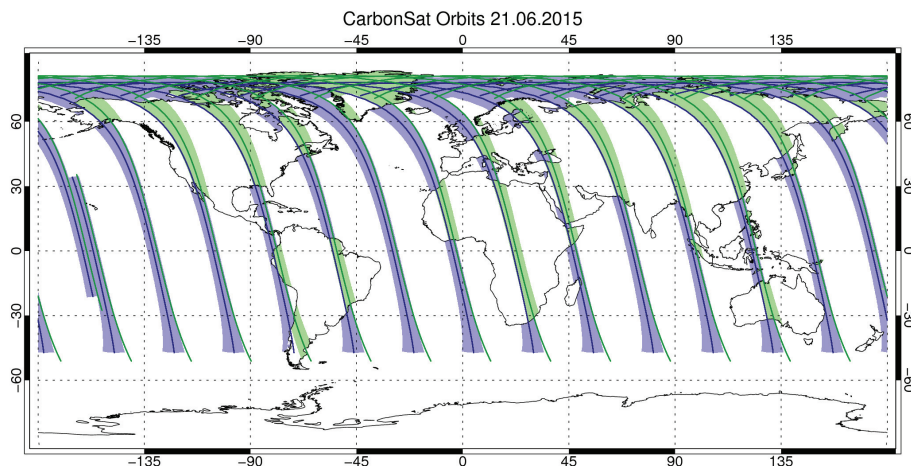


Fig. 4. CarbonSat orbital coverage for one day (21 June 2015) assuming a swath width of 500 km corresponding to 250 across-track ground pixels of width 2 km each. Over land the main mode is the nadir mode (the coverage is shown in green) and over water the sun-glint mode (blue). All ground pixels on the day side are included up to a solar zenith angle of 80°.

Title Page

Abstract

Introduction

Conclusions

References

Tables

Figures

◀

▶

◀

▶

Back

Close

Full Screen / Esc

Printer-friendly Version

Interactive Discussion



**Monitoring CO₂
emissions from
space**

H. Bovensmann et al.

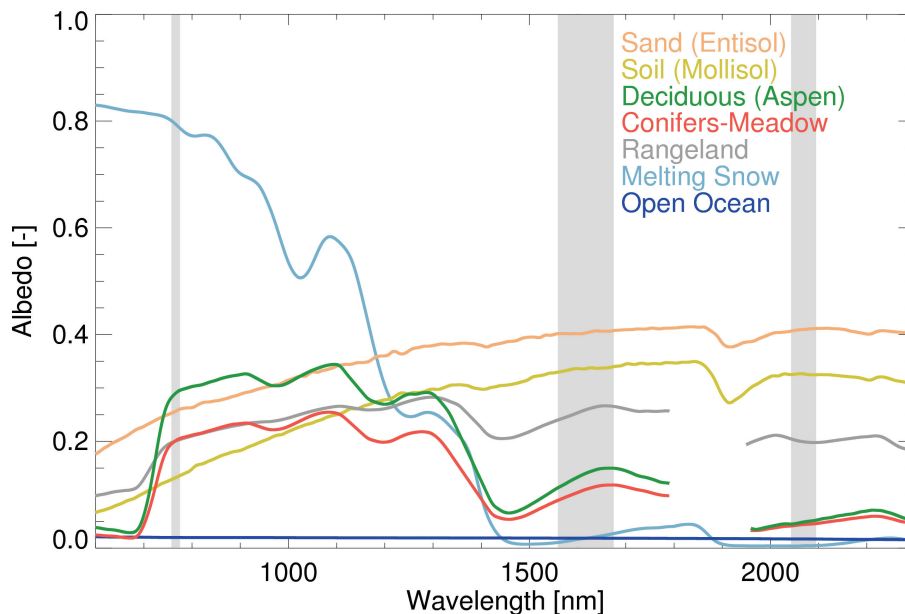


Fig. 5. Spectral albedos of different natural surface types. The shaded vertical regions indicate the spectral positions of the three CarbonSat spectral bands. The spectral albedos are reproduced from the ASTER Spectral Library through courtesy of the Jet Propulsion Laboratory, California Institute of Technology, Pasadena, California (copyright 1999, California Institute of Technology) and the Digital Spectral Library 06 of the US Geological Survey.

[Title Page](#)[Abstract](#)[Introduction](#)[Conclusions](#)[References](#)[Tables](#)[Figures](#)[◀](#)[▶](#)[◀](#)[▶](#)[Back](#)[Close](#)[Full Screen / Esc](#)[Printer-friendly Version](#)[Interactive Discussion](#)

Monitoring CO₂
emissions from
space

H. Bovensmann et al.

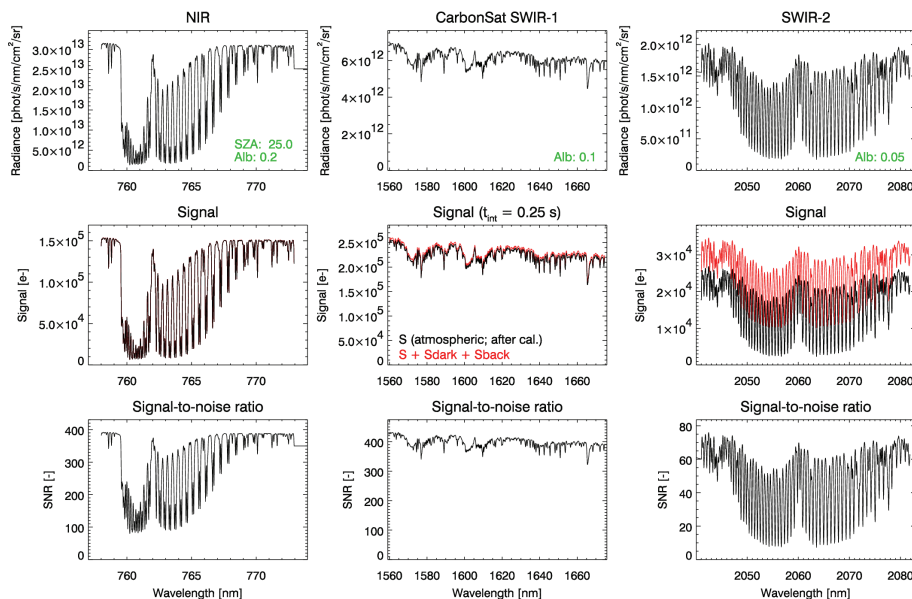


Fig. 6. Results of the CarbonSat instrument simulation for the VEG₂₅ scenario (albedo: vegetation, SZA 25°) for an integration time of $t_{\text{int}}=0.25$ s. Top: Radiance spectra in the three spectral bands covered by CarbonSat. Middle: corresponding signal (in electrons; red: before calibration; black: after calibration, i.e., after subtraction of detector dark and thermal background radiation signals). Bottom: corresponding signal-to-noise ratio.

Title Page

Abstract

Introduction

Conclusions

References

Tables

Figures

◀

▶

◀

▶

Back

Close

Full Screen / Esc

Printer-friendly Version

Interactive Discussion



**Monitoring CO₂
emissions from
space**

H. Bovensmann et al.

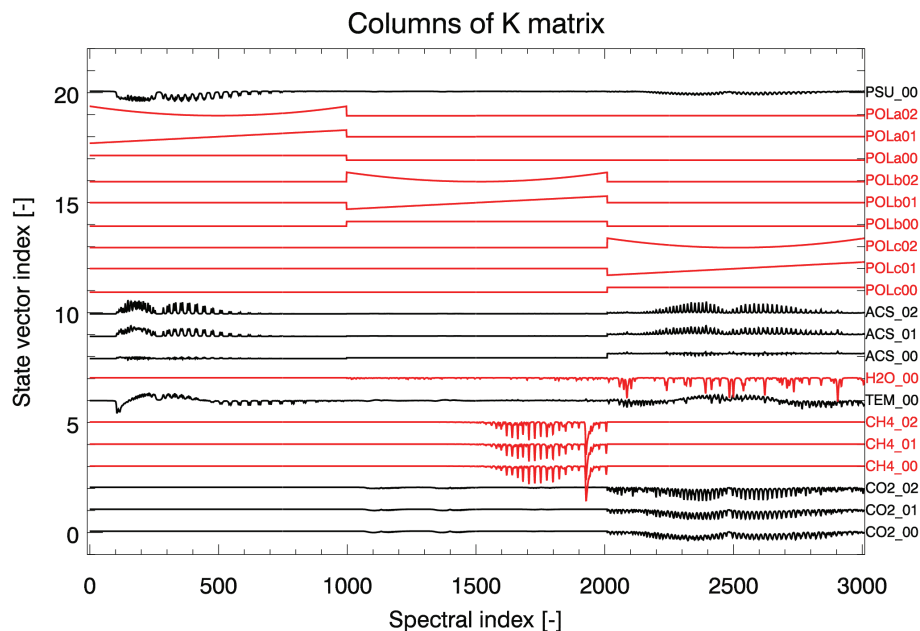


Fig. 7. Visualization of a typical retrieval Jacobian (**K**) matrix. Each spectrum shows the (scaled and shifted) derivative of the logarithm of the sun-normalized radiance due to a change of the corresponding state vector element. The state vector element identifiers are shown on the right hand side. For an explanation of the state vector elements see main text and Table 4.

[Title Page](#)[Abstract](#)[Introduction](#)[Conclusions](#)[References](#)[Tables](#)[Figures](#)[◀](#)[▶](#)[◀](#)[▶](#)[Back](#)[Close](#)[Full Screen / Esc](#)[Printer-friendly Version](#)[Interactive Discussion](#)

CO₂ vertical profiles

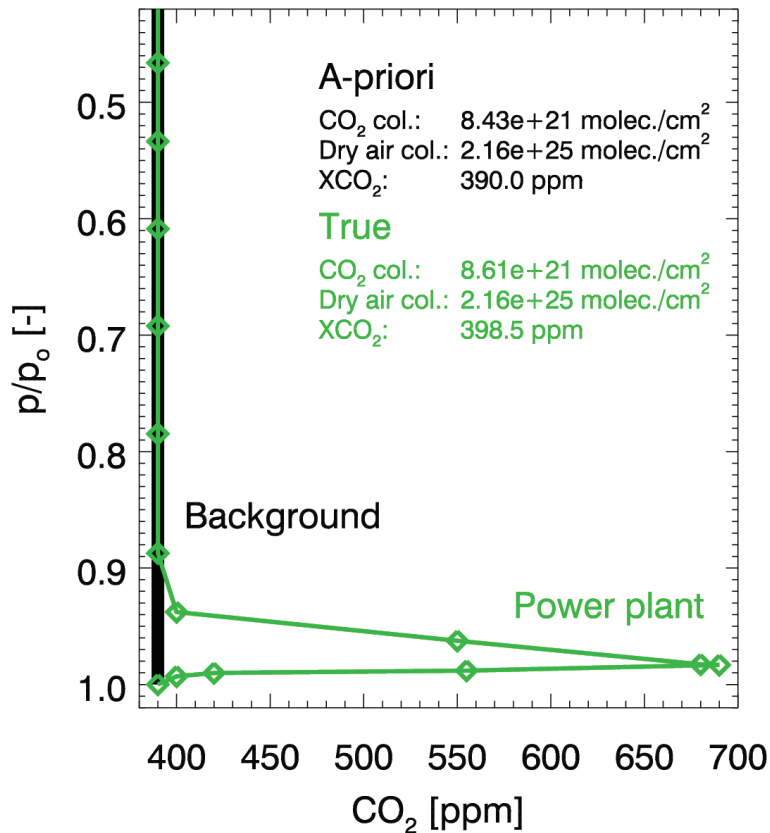


Fig. 8. A priori (black) and perturbed (green) CO₂ mixing ratio vertical profiles used for the simulated CarbonSat retrievals.

Title Page

Abstract

Introduction

Conclusions

References

Tables

Figures

◀

▶

◀

▶

Back

Close

Full Screen / Esc

Printer-friendly Version

Interactive Discussion



Monitoring CO₂
emissions from
space

H. Bovensmann et al.

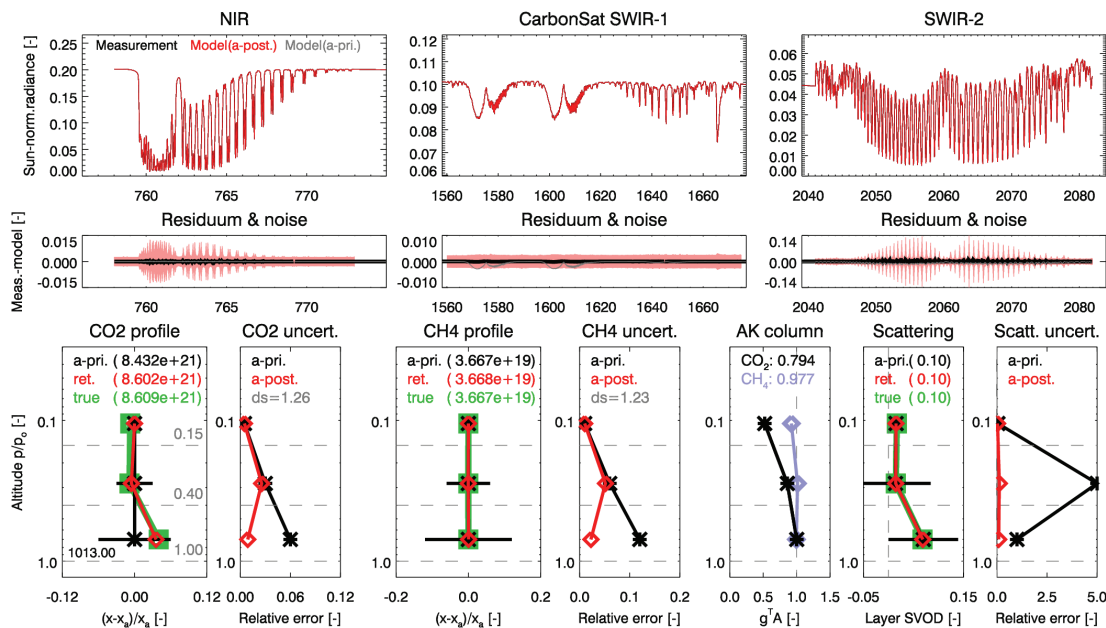


Fig. 9. Retrieval results for the VEG.25 scenario. Top: Sun-normalized radiance in the three CarbonSat spectral bands (three curves are plotted on top of each other but essentially only the red curve is visible). Middle: fit residuum (black line), i.e., relative difference between the simulated measurement and the fitted RT model (black). Also shown is the measurement error (light red) and the difference between the measurement and the simulated measurement before the fit (in grey; only clearly visible in the middle panel in the spectral regions covered by the two weak CO₂ spectral bands). Bottom: Vertical profiles of (from left to right) CO₂ and its uncertainty, CH₄ and its uncertainty, CO₂ and CH₄ vertical column averaging kernels, scattering layer vertical optical depth and uncertainty. The horizontal bars denote the uncertainties (1-sigma) in the three layers before (black) and after (red) the fitting procedure.

Title Page

Abstract

Introduction

Conclusions

References

Tables

Figures

◀

▶

◀

▶

Back

Close

Full Screen / Esc

Printer-friendly Version

Interactive Discussion



**Monitoring CO₂
emissions from
space**

H. Bovensmann et al.

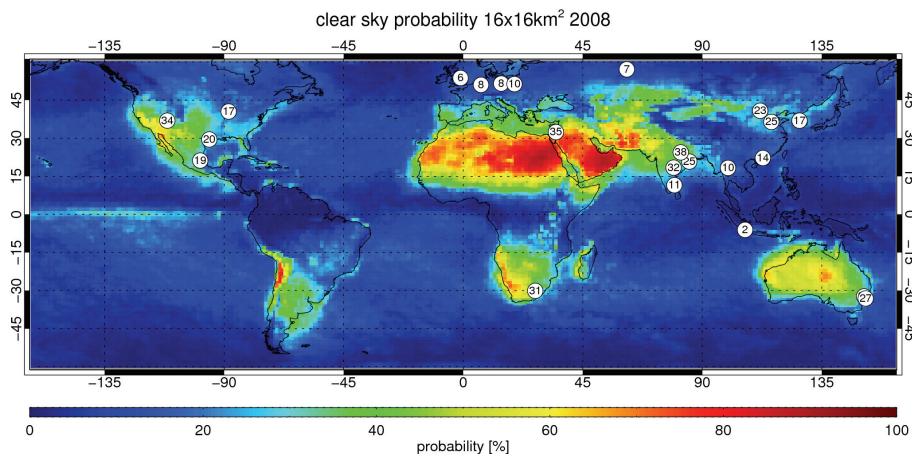


Fig. 10. Clear sky probability for $16 \times 16 \text{ km}^2$ large scenes for one year (2008) obtained from the MODIS/Aqua cloud mask data product. The white circles show the position of selected power plants (see also Table 6). The numbers in the circles show the numerical values of the clear sky probabilities in an area of $16 \times 16 \text{ km}^2$ around the power plants.

[Title Page](#)[Abstract](#)[Introduction](#)[Conclusions](#)[References](#)[Tables](#)[Figures](#)[◀](#)[▶](#)[◀](#)[▶](#)[Back](#)[Close](#)[Full Screen / Esc](#)[Printer-friendly Version](#)[Interactive Discussion](#)